



HAL
open science

Neogene sedimentation and tectonics in the Collón Curá basin (Patagonian Andes of Argentina)

Bertrand Nivière, Damien Huyghe, Cédric Bonnel, Pierre Lacan

► To cite this version:

Bertrand Nivière, Damien Huyghe, Cédric Bonnel, Pierre Lacan. Neogene sedimentation and tectonics in the Collón Curá basin (Patagonian Andes of Argentina). *Journal of South American Earth Sciences*, 2019, 96, pp.102244. 10.1016/j.jsames.2019.102244 . hal-02399001

HAL Id: hal-02399001

<https://hal.science/hal-02399001v1>

Submitted on 20 Jul 2022

HAL is a multi-disciplinary open access archive for the deposit and dissemination of scientific research documents, whether they are published or not. The documents may come from teaching and research institutions in France or abroad, or from public or private research centers.

L'archive ouverte pluridisciplinaire **HAL**, est destinée au dépôt et à la diffusion de documents scientifiques de niveau recherche, publiés ou non, émanant des établissements d'enseignement et de recherche français ou étrangers, des laboratoires publics ou privés.



Distributed under a Creative Commons Attribution - NonCommercial 4.0 International License

1 **Neogene Sedimentation and Tectonics in the Collón Curá Basin (Patagonian Andes** 2 **of Argentina)**

3

4 Bertrand Nivière¹, Damien Huyghe², Cédric Bonnel¹ and Pierre Lacan³

5 ⁽¹⁾ Université de Pau et des Pays de l'Adour, Laboratoires des Fluides Complexes et leurs Réservoirs, CNRS

6 UMR 5150, Avenue de L'université, Pau, France

7 ⁽²⁾ MINES Paris Tech, PSL University, Centre de Géosciences, 35 rue St Honoré, 77305 Fontainebleau Cedex,

8 France

9 ⁽³⁾ Centro de Geociencias, Universidad Nacional Autónoma de México, Blvd. Juriquilla, 3001, 76230, Juriquilla,

10 Querétaro, México

11

12 **Keywords**

13 Collón Curá basin; Neogene Basin; ⁴⁰Ar/³⁹Ar dating; Intramontane basin; Patagonian Andes; plate
14 kinematics; subduction.

15

16 **ABSTRACT**

17 We recall here recent developments concerning the filling and paleogeography of the Neogene Collón Curá
18 basin in the foothill of the North Patagonian Andes. To better constrain its evolution, we bring two new
19 ⁴⁰Ar/³⁹Ar on biotite datings of two ignimbrites that allow bracketing of the filling between 19.04 ± 0.72
20 and 5.06 ± 0.69 Ma. Like the other intramontane basins of the North Patagonian foothill, the Collón Curá
21 basin initiated around 18 Ma at the time of the Quéchuá phase. This corresponds in the area neither to an
22 increase of the convergence rate of the Nazca and South America plates, nor to a significant change in the
23 angle of convergence. We propose to look at this profound alteration of the regional stress regime in the
24 light of the recent results of analog and numerical modeling of subduction. Folding of the slab above the
25 mantle discontinuity at 660 km depth leads to the development of geometries that we retrieve in seismic
26 tomography images in the region. Modeling shows that the overriding plate is coupled to this folding in
27 depth. It suffers from changes in stress (from extensive to compressive stress regime) and topography. It
28 is assumed that a more compressive stress regime will favor the reactivation of border faults of the basin
29 and a regional uplift, hence agradation in basins. On the contrary, subsidence associated with a decrease

30 in shortening will favor the backward erosion that will cannibalize these basins. The life duration of basins
31 will be modulated by efficiency of earth surface processes proper to each watershed (catchment area,
32 river slopes, lithology...). This internal cyclicity of subduction due to slab folding is freed from the
33 kinematics of convergence. It is now necessary to look for the expression of this process in the sequential
34 filling of the basins.

35

36 **Introduction**

37 As for the Neuquén Andes to the north (e.g. Branellec et al, 2015; Branellec et al, 2016), the Neogene
38 reactivation of basement heterogeneities resulted in the North Patagonian Andes to the generation of an
39 array of partitioned basins surrounded by basement highs (Figure 1; Mosquera and Ramos, 2006; García
40 Morabito et al., 2011; García Morabito and Ramos, 2012; Huyghes et al., 2015a). Some of these basins have
41 an Oligocene extensional history and they have been subsequently inverted during the Miocene (e.g.
42 Ñirihuaú basin, Paredes et al., 2009; Cura Mallín Basin, Folguera et al., 2006; Kilca-Aluminé Basin,
43 Franzese et al., 2011; Auca Pan Basin, Ramos et al., 2015). The Collón Curá basin is one of these Miocene
44 basins. It is a small basin (<5000 km²) that currently contains no more than 350 m of Neogene sediments
45 and these sediments are being excavated. It does not present the economic resources of its huge neighbor,
46 the Neuquén basin. It is a fault-bounded intramontane basin integrated in the thrust belt (García Morabito
47 et al., 2011) and formed behind an actively growing topography. Here is one of its geological interest, it is
48 an important recorder of the Miocene deformation, erosion, and syntectonic deposition.

49 The stratigraphic framework is now laid out in broad outline as well as the main stages of its
50 paleogeographic evolution (e.g. Huyghes et al., 2015a). We recall the main lines at the beginning of the
51 paper. But recent discussions show that the chronological framework remains to be consolidated
52 (Franzese et al., 2018). This is why we present here two new absolute dating of ignimbrites at the top and
53 at the base of the outcropping Miocene sedimentary filling in order to better constrain the period of
54 activity of the basin.

55 The Collón Curá basin is an intra-mountain basin above an active margin and tectonics has potentially
56 played a determining role in its evolution. Significant progress has been made in recent years in
57 understanding the dynamics of subduction when the slab is encountering the mantle discontinuity at 660
58 km in depth. Analog modeling first and then numerical approaches specified the folding of the slab above

59 this discontinuity. They characterized the durations of the process and evaluated how it forced shallow
60 uplift and stress (e.g. Guillaume et al., 2009, Gibert et al., 2012, Cerpa et al., 2014, 2015). In parallel,
61 seismic tomography imagery returned in the area geometries that resemble the modeled geometries
62 (Pesicek et al., 2012). Slab break-off had already been invoked to comment the evolution of the basin (e.g.
63 Ramos et al., 2014b). We propose to include it as an element of a broader scheme of analysis that could
64 open (or not) a new way of interpretation of the regional dynamic.

65 We will therefore pursue three main goals here. Given the expectations of this issue, we will first focus on
66 the Neogene infill and stratigraphic framework of the basin. We then consolidate the timing of the basin
67 with two new dating of ignimbrites. At least, the final discussion is speculative. It proposes to extend
68 interpretations already advanced on the link between subduction and the dynamics of the basin. One may
69 wonder if this evolution is not partially decoupled in time from the global kinematics.

70

71 **Regional Setting**

72 We focus on an area located south of the Huincul Ridge that is a east-west inverted fault zone
73 corresponding to a structural high formed after the Jurassic in the south of the Neuquén basin (Mosquera
74 and Ramos, 2006; Grimaldi and Dorobek, 2011; Naipauer et al., 2012; Figure 1). This part can be divided
75 into four main morpho-structural domains corresponding from west to east to (1) the Main Cordillera, (2)
76 a series of several NNW-SSE oriented depocenters on the borders of the relief, (3) a nearly north-south
77 continuous topographic high and (4) the Picun Leufu basin that corresponds to the main foreland.

78 The depocentres individualized east of the main cordillera correspond from north to south to the Kilca-
79 Aluminé depocenter, the Auca Pan and Catán Lil depocenters and the Collón Curá basin, which is the most
80 important one in the study area (Figure 1). The Kilca-Aluminé and Collón Curá depocenters have been
81 interpreted as extensive depocenters during the Oligocene and lower Miocene and were filled at that time
82 by volcanic and volcano-sedimentary deposits corresponding to the Auca Pan Formation in the Collón
83 Curá Basin (Vergani et al., 1995; Franzese et al., 2011; García Morabito and Ramos, 2012). These basins
84 have been inverted since the middle Miocene in response to the establishment of the Quechua
85 compressive phase (Pardo-Casas & Molnar, 1987; Cobbold & Rossello, 2003; García Morabito et al., 2011;
86 Huyghe et al., 2015a). Thus, due to this shift toward a compressive regime, these depocenters were
87 isolated from the rest of the foreland by the inversion of Triassic normal faults (D'Elia et al., 2012) and the

88 uplift of basement blocks corresponding to the Sañico Massif, prolonged to the north by the Catán Lil
89 anticline (Ramos et al., 2014b). Thus, the Collón Curá, Kllka and Catán Lil basins became – at least partially
90 – endorheic during most of the Neogene and were filled by the erosional products of the main cordillera
91 and by volcanic and volcano-sedimentary deposits (García Morabito et al., 2011; Huyghe et al., 2015a). In
92 particular, the Collón Curá basin was partially isolated from the Picun Leufu basin from ~11 to 8 Ma due
93 to the onset of the uplift of the Sañico massif and was probably fully endorheic until the Late Pliocene (~3
94 Ma) when the drainage network reconnected to the Picun Leufu basin (Huyghe et al., 2015a). After that,
95 erosion predominated in the Collón Curá Basin and Huyghe et al. (2015b) suggested that compression was
96 pushed to the east of the Sañico Massif near the Pampa Curacó Plateau during the Pliocene. Although Plio-
97 Quaternary deformation processes have been documented in the Chihuidos and Anelo area farther north
98 (Messenger et al. 2010), a continuation of shortening up to the present day is still a matter of debate,
99 particularly across the foreland of the North Patagonian Andes, where evidence of continuing shortening
100 during the Quaternary is scarce and ambiguous.

101 The Neogene sedimentary filling is then unequally distributed in the study area. The Collón Curá basin
102 with a maximum thickness of 500 m (García Morabito et al., 2011) is the main depocenter. The Picun
103 Leufu area only preserves small relicts of Neogene syn-compressive deposits on topographic highs
104 (Huyghe et al., 2015a).

105 North (the Cura Mallin and Agua Amarga basins) and south of the study area (the Nirihuau and Gastre
106 basins) are the largest Neogene intermontane basins of the foothill and of the mountain interior (Figure
107 1). The Cura Mallin and the Nirihuau basins preserve above Oligocene extensional deposits, several
108 kilometers of syn-synorogenic Neogene deposits (Bechis & Cristallini, 2005; Bechis et al., 2014 ; Paredes
109 et al., 2009; Orts et al., 2012).

110

111 **Miocene Depositional History of the Collón Curá Basin**

112 At the bottom of the basin filling, the **Auca Pan Formation** is made up of andesitic rocks related to a
113 magmatic event from 36 to 43°S that took place between 33 and 20 Ma in the retroarc zone of the foreland
114 system (Figures 2 and 3; Turner, 1965, 1973; Rapela et al., 1983; Lagorio et al., 1998; Franzese et al.,
115 2011; Ramos et al., 2014b). It was deposited in extensive depocenters at the feet of the main cordillera.

116

117 The **Collón Curá Formation**. The Collón Curá Fm is exposed along rivers of the eastern margin of the
118 basin at the border of the Sañico Massif and along the Rio Limay in the southern part of the basin (Figure
119 2). The pioneering work by Roth (1899) identified the formation later named by Yrigoyen (1969). Based
120 on its mammal fauna, Roth (1899) attributed it to Middle Miocene and Pascual and Odreman Rivas (1971)
121 re-evaluated this attribution as Middle to Late Miocene.

122 Absolute ages came with K/Ar radiometric dating of pyroclastic deposits that yielded ages of 15.4 ± 0.3 Myr
123 and 14 ± 0.3 Myr (Marshall et al., 1977) and 11 ± 1 Myr (González Díaz & Nullo, 1980). At the base of the
124 formation, the Pilcaniyeu Ignimbritic Member was dated at 15 Myr by Rabassa (1975) and 13.8 ± 0.9 Myr
125 by Mazzoni & Benvenuto (1990). Above it, Cazau et al. (1989) obtained an age between 11.5 and 10.7 Myr
126 at the base of the clastic deposits.

127 In the Collón Curá basin, Giacosa et al. (2001) attributed to the Langhian and Serravalian the Collón Curá
128 Fm. but the upper boundary is not consistently defined.

129
130 The Collón Curá Fm. is rarely exposed in the Collón Curá basin. To the north of the basin, it exhibits an
131 angular unconformity with the underlying Paleogene Auca Pan Fm. The formation is thin, its basal part
132 consists of a 20 m thick ignimbrite. This pyroclastic flow grades vertically into 5 m of sandstones with
133 igneous rock pebbles. Sedimentary facies correspond to tuffaceous deposits, mostly reworked by fluvial
134 processes, showing channels larger than 5 m, alternating with primary volcanosedimentary deposits
135 (Figure 3, section C).

136

137 **Caleufú Formation**. The middle and upper Neogene Caleufú Formation consists of the Limay Chico and
138 Alicura members (González Díaz et al., 1986) that comprises the vast majority of Neogene strata in the
139 basin.

140 González Díaz et al. (1986) shed new light on the stratigraphic framework of the Collón Curá basin. They
141 named Caleufú Fm the sediments overlying the tuffaceous material of the Collón Curá Fm that were
142 formerly known as the Rio Negro Fm and the Alicura Fm (Dessanti, 1972; Nullo, 1979; González Díaz &
143 Nullo, 1980). The Chimehuin Fm of Turner (1973) included the Collón Curá Fm and the grey sandstones
144 (Galli, 1954) of the present Limay Chico Mb of González Díaz et al. (1986). The question was about the
145 number of aggradational cycles recorded by these series. Invoking a single aggradational sequence from
146 sedimentologic arguments, González Díaz et al. (1986) regrouped the Río Negro and Alicura Fm into a

147 single unit, the Caleufú Fm, which they divided into two members.
148 If Nullo (1979) ascribed the formation to the Middle Pliocene by analogy with the Río Negro Fm in its type
149 locality, Nullo (1979) and González Díaz & Nullo (1980) nevertheless placed in the Pleistocene the Alicura
150 Member. A partial chronologic framework is given by K/Ar dating of ignimbrites and basalt flows. Basalts
151 at the base of the Limay Chico Mb yield an age of 20 ± 4 Myr and two ignimbrites in the middle of the
152 formation, ages of 14 ± 1 Myr (González Díaz et al., 1990). The top of the Limay Chico Mb is given by
153 another ignimbrite dated at 8 ± 2 Myr (González Díaz et al., 1990). The 3 ± 0.5 Myr Tipilihuqué basalt flow
154 that covers the Alicura Member, gives the upper bound of the Caleufu Fm (González Díaz et al., 1990). But
155 this framework remains to be consolidated especially for its basal part where these ages overlap those
156 obtained for the Collón Curá Fm (e.g. Rabassa, 1975; Mazzoni & Benvenuto, 1990; or Cazau et al., 1989).
157 Another question is whether or not the ignimbrite at the top of the Limay Chico Mb (8 ± 2 Myr; González
158 Díaz et al., 1990) corresponds to the Chimehuin Ignimbrite dated by Mazzoni & Rapela (1991). Moreover
159 the age of 3 ± 0.5 Myr obtained by González Díaz et al. (1990) does not strictly date the end of the
160 aggradation of the Alicura member. In the Las Coloradas basin which is located northeast of the Collón Curá
161 basin, Franzese et al. (2018) dated to 8.5 Myr ($^{39}\text{Ar}/^{40}\text{Ar}$ age) the Tipilihuque basalt that toplaps the
162 Miocene infill of this basin. In the field the lava flow does not overlap the Alicura member but its
163 southernmost remnants are very close to the basin closure. So this arrangement raises questions about
164 the actual age of the end of aggradation in the Collón Curá basin. We will come back to this point later on in
165 the paper.
166
167 The Caleufú Fm consists of siliciclastic and volcanosedimentary material. Dominant lithologies correspond
168 to clay, sand and coarse sands in the lower part of the formation and grades up in the upper part where
169 coarse conglomerates become more prevalent (Figure 3).
170 The Limay Chico Mb usually shows grey sandstones, tuffaceous deposits, conglomerates and claystones.
171 Centimetre- to decimetre-sized clasts derived from Cenozoic and Mesozoic volcanic sources and from
172 Paleozoic plutonic rocks. Pumice fragments with a greyish colour are abundant and frequent cross-
173 bedding indicates a fluvial depositional environment. Laterally, the Limay Chico Mb. is made up of grey
174 sandy pumice-rich fluvial deposits with the occurrence of red pebbles of igneous rocks, frequently at the
175 base of fining-upward sequences.
176 Above the Limay Chico Mb in the middle of the basin, the Alicura Mb is composed of conglomerates with

177 sandstones and tuffaceous intercalations. Nature of clasts remains unchanged as well as lithologies. The
178 transition with the Limay Chico Mb is difficult to locate (González Díaz et al., 1986). Red pebbles of
179 igneous rocks are locally observed along the western border of the basin, frequently at the base of fining-
180 upward sequences (Huyghe et al., 2015a).

181 A spectacular 130 m thick white ignimbrite is intercalated within the Caleufú Fm at the north east of the
182 basin (Figure 3, section A). This unit is completely homogeneous and shows abundant quartz and pumice
183 content. Another thinner ignimbrites (only a few meter thick) have been preserved in the basin
184 particularly at the top of the series.

185

186 Pampa Curacó Formation

187 These facies are interpreted to have been deposited in fluvial environments, with some lacustrine events
188 (Escosteguy & Franchi, 2010) and several paleogeographic settings have been proposed. It would record
189 the growth of the orogenic front (González Díaz et al., 1986) or could have a fluvio- glacial origin (Gracia,
190 1958; Galli, 1969; González Díaz & Nullo, 1980). Alternatively, Flint & Fidalgo (1968) postulated that it
191 corresponds to a pediment.

192

193 **Time Bracketing of the Collón Curá Infill**

194 The sedimentary filling of the basin where it can be observed, rests on different formations which extend
195 from the Triassic in the south to the Oligocene elsewhere and even on the crystalline basement. This lack
196 of stratigraphic concordance does not allow an easy assignment of the age of the basin. The authors have
197 therefore endeavored to characterize their faunistic content (see above). Dating of tephra in conjunction
198 with stratigraphic relations had been performed to better constrain the ages of geomorphic units.

199 These dates did not contradict the first assignments but they nevertheless raise in the current context
200 some difficulties. The first is documentary. Most often published in symposium proceedings, they are
201 hardly accessible for the time being to the international community. In addition, these often old datings do
202 not always allow the reader to locate accurately the dated samples geographically and stratigraphically.

203 Authors implemented two methods, K-Ar ou $^{40}\text{Ar}/^{39}\text{Ar}$, most often (it seems to us) on whole-rock samples
204 (e.g. Marshall et al., 1977; Mazzoni & Benvenuto, 1990). The current reader cannot evaluate if former
205 workers neglected or not uncertainty in nucleogenic interference corrections in defining a plateau. This is

206 strictly valid only when a sample is compositionally homogenous (Renne, 2000). This is frequently untrue
207 in the case of whole rock basalts and therefore interference corrections should be included in the
208 definition of the plateau. Pyroclastic rocks too should be always suspected of containing xenocrystic
209 contaminants and should never be analyzed as a whole-rock sample. Highly vesicular lavas, scorias, and
210 pumices are problematic because their high surface to volume ratio causes excessive adsorption of
211 atmospheric Ar which may overwhelm $^{40}\text{Ar}^*$. So whole-rock K-Ar dates are increasingly suspected of being
212 systematically too young (e.g. Mc Dougall et al., 1992; Renne et al., 1993).

213

214 We chose to date individual crystals of biotite sampled in ignimbrites of the Collón Curá and Caleufú
215 formations. One of the most profound advantages of this approach is that pyroclastic material such as
216 crystal-bearing tuffs can be dated without danger of bias from xenocrystic contamination (e.g. Curtis,
217 1966; Lo Bello et al., 1987; Deino et al., 1990). Moreover $^{40}\text{Ar}/^{39}\text{Ar}$ incremental heating analysis of biotite
218 presents significant advantages because the proportion of atmospheric ^{40}Ar is typically reduced in higher
219 temperature steps. For volcanic biotites, a $^{40}\text{Ar}/^{39}\text{Ar}$ plateau is generally a sufficient criterion for
220 reliability.

221 So, we sampled two thick ignimbrites located at the base of the Collón Curá Formation (Figure 3; base of
222 section C of Huyghe et al., 2015a; S $40^{\circ}10.27'$, W $70^{\circ}39.39'$) and at the top of the Alicura Member of the
223 Caleufú Formation (top of section B of Huyghe et al., 2015a; S $40^{\circ}07.121'$, W $70^{\circ}55.212'$ location in Figure
224 2). We sampled 5 kg of these ignimbrites rich in pumices and biotites. Samples were taken at ~ 1 m
225 depth to avoid potential surface alteration of the biotites. The plateau date has been calculated as the
226 inverse variance weighted mean of individual plateau step ages. The uncertainty derived from error
227 propagation (e.g. Renne et al., 1996).

228

229 The basal ignimbrite in the Collón Curá Formation yields an age of 19.04 ± 0.72 Ma and the top one in the
230 Caleufú Formation, an age of 5.06 ± 0.69 Ma (Figures 4 and 5 and Table 1). Compared to the stratigraphic
231 synthesis these ages provide new direct constraints of the history of the CCB. First, it moves the base of
232 the Collón Curá Formation and the top of the Auca Pan Formation from 16 to 19 Ma compared to the
233 stratigraphic framework proposed by Huyghe et al. (2015a) (Figure 4). The age boundary between these
234 two formations was not accurately dated and this new age brings strong constraints about its age.

235

236 The age of the top of the sedimentary filling of the basin is subject to several controversies (see the
237 synthesis of Huyghe et al., 2015a) and ranges between 8 and 3 Ma according to the authors and the dating
238 method (Nullo, 1979; González Díaz and Nullo, 1980; González Díaz et al., 1990; Mazzoni & Rapela, 1991).
239 Here, the absolute dating of the ignimbrite allows a time constrain of 5 Ma for the end of the filling of the
240 basin (Figures 3 and 6).
241 These ages remain consistent with stratigraphic contains.

242

243 **Tectonic and Stratigraphic Evolution**

244 Huyghe et al. (2015a) considered four stages of paleogeographic evolution during the Neogene in this area
245 where shortening is supposed to be low (<10 km, Ramos et al., 2014a).

246 Prior to the Neogene filling of the basin, Eocene and Oligocene intervals are interpreted as a phase of
247 major erosion since Neogene deposits preserved to the east of the Sañico Massif often lie over Cretaceous
248 or Jurassic sediments with a reduced angular discordance (<5°) and seem to fill ancient paleovalleys
249 (Leanza et al., 1997; Hugo & Leanza, 2001). This evolution is characteristic of retro-arc foreland basins
250 (Jordan, 1995).

251 At the end of the Oligocene or at the beginning of the Miocene, sedimentation began along a nearly N-S-
252 oriented axis of maximum thickness deposition parallel to the Sañico Massif. The Collón Curá basin is
253 supposed to have been individualized since the end of the Early Oligocene (Ramos et al., 2014a) but in the
254 field, the oldest deposits are Early Miocene in age and are localized alteration products resulting from
255 erosion of the Oligocene volcanic Auca Pan Fm. (Figure 6A; Huyghe et al., 2015a). The North Patagonian
256 Massif (NPM) was probably not yet a prominent structure at that time.

257 In the Middle Miocene, a major volcanic phase supplied a large volume of volcanoclastic material to the
258 Collón Curá Fm. (Galli, 1969) that extended in the basin and in a wide surrounding area to the south, to
259 the east and up to the north of the NPM (Figure 6B). In the Picun Leufu basin, the same sedimentary
260 material displays channelized structures characteristic of a single fluvial system showing that the Sañico
261 Massif was probably not yet exhumed (Huyghe et al., 2015a).

262 Major change occurred during the Late Miocene and Early Pliocene. Progressive unconformities, with a
263 maximum dip of 13°, are observed within the Caleufú Fm. along the western margin of the Sañico Massif
264 in the central part of the Collón Curá basin (García Morabito et al., 2011). Many liquefaction structures,

265 interpreted as seismically induced and synsedimentary normal faults in the Limay Chico Mb. also show an
266 intensification of tectonic activity (Huyghe et al., 2015a). In the same time, the Picun Leufu basin to the
267 east is rather in non-deposition and possible erosion. This segmentation of the deposits is a consequence
268 of the uplift of the Sañico Massif (García Morabito et al., 2011; Ramos et al., 2014a).
269 Thus, the Late Miocene Early Pliocene deposition is confined to an area of ca. 150 km by ca. 30 km in the
270 Collón Curá basin with a thickness of tens of meters east of the Sañico Massif while sedimentary thickness
271 reaches only few meters in the Renteria Plateau area to the east (Figure 2). Its connection with the rest of
272 the foreland remains questionable at this time; the Collón Curá basin might have been isolated from the
273 rest of the foreland basin. The deposition of the Limay Chico Member of the Calefú Fm. in the Picun Leufu
274 basin along the eastern border of the Sañico Massif suggests that it was rising and was eroded by rivers
275 flowing to the east. Nevertheless, given the reduced volume of relicts of the formation in the Picun Leufu
276 basin, if gateways existed during the filling of the Collón Curá basin, they were probably not active during
277 long periods. This observation shows that the uplift of the Sañico Massif was faster than the filling of the
278 Collón Curá basin, at least until the end of the deposition of the Calefú Fm.
279 The deposition of the Alicura Mb. of the Calefú Fm. during the Early Pliocene exhibits a coarsening
280 compared to the Limay Chico Mb. This may reflect the end of the major filling of the Collón Curá basin
281 (González Díaz et al., 1986) that was endoreic at this time (Huyghe et al., 2015a).
282 The Collón Curá basin underwent erosion during Late Pliocene and Early Pleistocene and the main
283 depositional area moved to the east. It is questionable whether regressive erosion began to affect the
284 Sañico Massif at this time and subsequently the Collón Curá basin, or if the activity of the surface
285 processes in the basin allowed its overflowing towards the Picun Leufu basin. There is a lack of any
286 sedimentological or morphological evidence to favor one or the other of these scenarios.

287

288 **Discussion**

289 **Timing of the basin in the foreland setting**

290 How the aggradational scheme of the basin highlights the mountain building processes in the area? The
291 question spans the temporal space when considering whether shortening prevails over a single prolonged
292 interval (~50–100 Myr) or over a series of punctuated events of shorter duration (<5–10 Myr) alternating
293 with episodes of neutral or extensional modes (e.g. Steinmann, 1929). It spans the spatial space when

294 questioning if individual pulses are restricted or not to particular segments of the Andean margin (e.g.
295 Groeber, 1951). It is why we choose to discuss the evolution of the Collón Curá basin compared to that of
296 its close neighbors, the Catán Lil and Agua Amarga to the north and the Ñirihuau–Collón Curá basin to the
297 south. These basins are the outermost Miocene intramontaine basins of the considered area.

298 Between 39°28′-39°48′ S and 70°29′-70°44′ W, the Catán Lil basin is a small intermontane basin (40x20
299 km) that accumulated 400 m of sediments during the Miocene (García Morabito et al., 2011; Figure 1).
300 Developed between two thick-skinned anticlines, it nests above a Paleozoic crystalline basement where a
301 Mesozoic continental–marine sedimentary succession forms the southernmost part of the Neuquén Basin
302 (Figure 2). Farther to the north, the Agua Amarga basin also developed above the Mesozoic infill of the
303 Neuquén basin but to the north of the Huincul ridge, a strong inherited transverse structure that delimits
304 the southern limit of the Neuquén basin (Figure 1). The Agua Amarga basin is larger (80x20 km) but not
305 thicker than the Collón Curá basin and is located at the toe of the thin-skinned domain of the Agrio fold-
306 and-thrust-belt and west of the thick-skinned Chihuidos anticlines. Compared to the northernmost basins,
307 the Ñirihuau–Collón Curá basin at south of the Collón Curá basin, is larger (200 x 40 km; Figure 1). With
308 more than 2000 m of Late Oligocene to Middle Miocene sediments deposited on top of the Oligocene
309 volcanic rocks of the Ventana Formation (Rapela et al., 1988) and the igneous-metamorphic rocks of the
310 Cushamen Formation (Volkheimer, 1964), it is also thicker (Spalletti, 1981; González Bonorino & González
311 Bonorino, 1978). It has been alternately interpreted as a pull-apart basin (Spalletti & Dalla Salda, 1996), as
312 an extensional basin in a back-arc setting (Mancini & Serna, 1989; Cazau et al., 1989) and as a foreland
313 basin (Ramos & Cortés, 1984; Giacosa & Heredia, 1999 ; Bechis et al., 2014).

314

315 Did shortening prevail over a single prolonged interval or over a series of punctuated events of shorter
316 duration? This makes necessary to set the chronological framework of these basins with the reserve
317 imposed by the partial knowledge that we have of these basins. We dated two ignimbrites at the base and
318 top of the sedimentary filling of the Collón Curá basin. At the bottom of the infill outcropping to the heart
319 of the basin at the base of the Collón Curá Formation, we obtained an age of 19.4 ± 0.72 Ma (Figure 5). This
320 dating allows revising the former ages by Rabassa (1975), Marshall et al. (1977) and Mazzoni &
321 Benvenuto (1990) that yielded younger ages comprised between 13 and 16 Ma. So subsidence of the basin
322 occurred a little bit earlier than the age given by Huyghe et al. (2015a). But this age does not correspond
323 to the onset of sedimentation in the basin because the base of the basin is still buried.

324 The bottom of the Catan Lil basin is comprised between 16.1 and 13.8 Ma (Figure 7; Marshall et al., 1977;
325 Rabassa, 1978; Rapela et al., 1988; Mazzoni & Benvenuto, 1990; Orts et al., 2012; Bilmes et al., 2013, 2014;
326 Ramos et al., 2014a, 2015). The bottom of the sedimentary infill outcrops in the Agua Amarga basin. It is
327 the Puesto Burgos Formation (Hugo & Leanza, 2001) late Oligocene-early Miocene in age (Figure 7). The
328 sedimentary history began in the Ñirihuau basin at the same time with deposition of the marine Ñirihuau
329 Formation (Roth, 1922 ; González Bonorino, 1973) that opened towards the Pacific (Figure 7). Cazau et al.
330 (2005) and Paredes et al. (2009) revised the stratigraphic frame of the formation. More important here is
331 the transition from lacustrine to fluvial deposition that occurred at the top of the Ñirihuau formation
332 around 17 Ma and signed the onset of tectonic inversion (Paredes et al., 2009). So the onset of these
333 basins as intra-mountainous basins occurred in a relatively narrow time bracket centered around 18 Ma
334 (± 1 Ma).

335 Sampled at the top of the Collón Curá Formation, the upper ignimbrite gives us the end of aggradation at
336 about ~ 5 Ma (Figure 5). On the basis of the bibliographic data, Huyghe et al. (2015a) previously assigned
337 it to a little over 3 Ma. In the close Catán Lil basin, Franzese et al. (2018) dated plagioclases ($^{39}\text{Ar}/^{40}\text{Ar}$) of
338 a lava flow of the basaltic plateau at top of the sedimentary infill that was assigned to the Plio-Quaternary
339 (Cucchi & Leanza, 2005; Rojas Vera et al., 2014). They obtained an older age of ~ 9 Ma, in agreement with
340 the $^{39}\text{Ar}/^{40}\text{Ar}$ age of the upper basaltic unit in the Kilca-Aluminé basin (Franzese et al., 2011, Figure 7). So
341 aggradation in the basin ended earlier than expected and this allows these authors to postulate that
342 shortening did not continue in the area after the end of the Miocene. Nevertheless our dating in the Collón
343 Curá basin shows that volcanic activity continued until the Pliocene what supports the interpretations by
344 Ramos et al. (2014a) and Huyghe et al. (2014, 2015). Franzese et al. (2018) did not sample the youngest
345 flow of the basaltic plateau. Farther north in the Agua Amarga basin, the Pampa Encima Formation
346 constitutes the last interval of aggradation before a drop of the base level of the Rio Neuquén and Rio
347 Agrio (Hugo & Leanza , 2001; Messenger et al., 2010). It was deposited during the Pliocene (Leanza and
348 Hugo, 2001). Similarly to the Collón Curá basin, the final stage of the Ñirihuau basin contains pyroclastic
349 and volcanoclastic materials reworked by fluvial and aeolian processes until Early-Late Miocene
350 (Langhiane–Tortoniane; Giacosa et al., 2001). Comprised between ~ 10 and ~ 5 Ma, the time window
351 spanning the onset of the excavation of these basins is larger.

352

353 The Miocene history of these basins is that of intra-mountainous basins. On the basis of bibliographic data,

354 the aggradation in these basins located between 37 and 40 ° S over more than 300 km began on a rather
355 narrow window of time centered around 18 Ma. It coincides to the west with the closure of the Traigen
356 oceanic basin between 20 and 15 Ma (Folguera et al., 2018). These features (timing and geographic
357 distribution) suggest that we entered at this time under dynamic conditions that allowed the
358 segmentation of the foreland by localized uplifts, it is the Quechua phase of the authors (e.g. Steinmann et
359 al., 1929).

360 The end of the aggradation in these basins spreads over a longer period of 5 Ma. Field observations show
361 active crustal folding of the Chihuidos and Sauzal folds east of Agua Amarga basin (Messenger et al., 2010)
362 and along the eastern border of the San Rafael block (northern Neuquén Basin) which is inverting since
363 the Late Miocene (Costa et al., 2006, Folguera et al., 2018; Branellec et al, 2016). On the basis of these
364 observations, the Quechua phase would continue until the late Pleistocene at north of the Collón Curá
365 basin.

366 The development along the Neuquén River of an alluvial fan at the outlet of the Agua Amarga basin shows
367 that reconnection of the basin with its foreland has been achieved by backward erosion which then
368 initiated the excavation of the basin. If backward erosion is of course controlled by the activity of the
369 tectonic dam, it is also modulated by the intensity of surface processes determined by external forcing
370 (climate, lithology, watershed geometry; e.g. Hilley and Strecker, 2005). These factors could therefore
371 spread the timing of the basin excavation over time according to local characteristics.

372 However, Huyghe et al. (2015a) showed that the Collón Curá basin was still subsiding when the foreland,
373 behind the tectonic dam, was already excavating. The vergence of the structure that initially isolated the
374 basin from its foreland is directed towards the basin. Its lithostatic load could drive a flexural subsidence
375 allowing for a time the activity of the basin.

376 The timing of initiation of these basins suggests that shortening controlled it at first order. The end of
377 aggradation spreads on a broader time window probably as the result of a stack of regional and local
378 forcings.

379

380 **Kinematic forcing on basin evolution**

381 Although the basins are distant from each other by several hundred kilometers, aggradation began in a
382 narrow time window (18+/-1 Ma). This suggests that a lithospheric forcing probably controlled it and we
383 examine here if the Atlantic spreading or if the conditions of the Pacific subduction can be linked to

384 shortening.

385

386 The growth of mid-oceanic ridges makes gravitational forces that could force the young and raised
387 oceanic lithosphere to slide down the weaker asthenosphere and push on lithospheric material farther
388 from the ridges (Meijer and Wortel, 1992). That is why the mid-Atlantic oceanic spreading could be a
389 potential tectonic forcing.

390 The geological marker does not show a lot of demonstrative evidence of the Peruvian phase of shortening
391 in the Collón Curá area because Cretaceous deposits are now eroded. But in the southern Neuquén basin,
392 the older macroscopic record of inversion we observed in the field is the discordance of the Huitrín
393 Formation above the folded Avilé sandstones west of Chos Malal. This shows that the onset of inversion
394 was Aptian in age. This is confirmed elsewhere in the basin by other observation or by seismic data (e.g.
395 Cobbold and Rosello, 2003; Grimaldi and Dorobek, 2011) and now by thermochronology (e.g. Sánchez et
396 al., 2017). This discontinuity follows shortly the onset of South Atlantic spreading at this latitude. Basing
397 on the age of the oldest magnetic record along the Atlantic margin of South America (e.g. 133 Ma at 39°S
398 and 120 Ma at 20°S; Meyer et al., 2017), kinematics models show that the Atlantic opening propagated
399 northward (Setton et al., 2012; Müller et al., 2018). It is especially interesting to note that the onset of
400 shortening in the Andes follows too this trend during the Cretaceous times: it begun at 125 Ma in the
401 southern Neuquén basin and only at 113 Ma in Peru (10°S; Margirier et al., 2017). So the mid-Atlantic
402 opening could play an operating forcing. The late Cretaceous inversion in Neuquén basin would be
403 unrelated for Chen et al. (2019) to the westward motion of South America because the magnitude of
404 displacement would be too low. But oceanic-opening and tectonic-shortening coincide in time and in
405 space.

406 The correlation does not work in the Miocene time. Indeed aggradation in the basins (i.e. shortening, 18
407 Ma) occurred when the mid-Atlantic spreading rate was steady at 37 and 40°S (Figure 8). For the Pacific
408 Ocean, the spreading rate decreased during this interval. It is not so surprising because ridge push is
409 mostly active in lithosphere younger than 90 Ma, after which it has cooled enough to reach thermal
410 equilibrium with older material and the slope of the lithosphere-asthenosphere boundary becomes
411 effectively zero.

412

413 The tectonic regime changes may be associated with other parameters as plates velocities, plates

414 directions, the absolute movement of the trench, the age of the oceanic plate, the presence of sediments or
415 the geometry of the oceanic plate (e.g., Ruff and Kanamori, 1983; Heuret et al., 2007; Schellart, 2008) that
416 is to say to the dynamics of subduction.

417 The westward shift of South America could have forced the inversion of the basin. Plate-tectonic
418 reconstructions show that South America did not stop migrating westward at the first order since the
419 opening of the South Atlantic Ocean (Setton et al., 2012; Müller et al., 2018; Gurnis et al., 2018). For the
420 period of time covered by the Collón Curá basin (0-18 Ma), is a change in the conditions of convergence
421 likely to initiate the onset of the Quechua phase? For the considered time window, the South America
422 plate continuously moved to the northwest and convergence angle between the Nazca and South America
423 plates did not change more than 25° (Figure 9 and 10). The onset of aggradation in the basins is coeval
424 with a decrease of the convergence rate between plates (Figure 10). It seems more “physical” to link the
425 onset of shortening with an increase of the convergence rate. Also it could be more reasonable to interpret
426 this inflexion in the convergence rate not as the cause of the occurrence of the Quechua episode but only
427 as an evidence of the increase of the coupling between both plates.

428
429 The inversion that occurred at 40°S without strong kinematic change, leads to look for another
430 explanations. The effect of the slab anchoring on the lower mantle interface and more generally the
431 modality of the penetration of the slab into the mantle above it, remains an under-explored way of
432 interpretation. The mantle retains a memory of subducted slabs, which body-wave tomography images in
433 situ as domains of faster-than-average seismic wave velocities. The rupture with at least 5 m of slip of the
434 M8.8 Maule earthquake in Chile in 2010 spreaded from 34 to 38°S (Lorito et al., 2011) and made it
435 possible to image it for the latitudes we are interested in (Figure 11; Pesicek et al., 2012). The first order
436 change in the slab geometry is located around 35°S with the transition from a horizontal Pampean flat
437 slab (at north) to a southern slab with a moderate dip of ~30°. At the latitudes of our study area, this
438 image does not show at the first order major differences between the north (section at 37°S) and south
439 (section at 39°S; Figure 11A). The slab normally dips up to 200 km. The anomaly then bends towards the
440 east and comes to horizontalization at a depth of 650 km. The slab, however, appears less continuous at
441 39°S and Pesicek et al. (2012) and Ramos et al. (2014) interpreted it as a result of slab tearing and
442 detachment at ~200 km in depth.

443 Another fast anomaly stands almost vertically below the subduction trench and reaches depths greater
444 than 1000 km (Figure 11A). This anomaly could also be interpreted as the remnant of a former slab diving
445 in the mantle as observed along the Pacific margin of North (e.g. Sigloch & Mihalynuk, 2013; Sigloch &
446 Mihalynuk, 2017) and South America (e.g. Pesicek et al., 2012; Chen et al., 2019). But its position may
447 surprise. Since the South American plate shifted continuously westwards since 125 Ma (Figure 9; e.g.
448 Seton et al., 2012), the trench shifted westwards too. So, we would be inclined to find the relics of the
449 ancient slabs further to the east below the American plate as observed farther to the north by Chen et al.
450 (2019). And the MITP08 tomography model too shows anomalies of seismic rates farther to the east that
451 could be interpreted as remnants of former slab segments (Li et al., 2008; Hosseini et al., 2018).

452 In detail, the image of Pesicek et al. (2012) at 37 ° S is emblematic (Figure 11A). The Wadati-Benioff plane
453 is associated with an anomaly of fast speeds which continues in depth up to 400 km. More than 200 km
454 away from the trench, the slab then stumbles on a thick anomaly of 350 km which continues until a depth
455 of 650 km . This one could correspond to a pile made by a slab folding on itself above the rheological
456 discontinuity of the mantle (Figure 11B and 13; e.g. Guillaume et al., 2009; Gibert et al., 2012; Sigloch &
457 Mihalynuk, 2013). The deep anomaly below the current slab shows an upward concave shape that must
458 be included in this pattern (Figure 11A). We propose at 39°S a scheme that involves first the shallow
459 rupture of the slab above 200 km in depth as invoked by Pesicek et al. (2012) and by Ramos et al.
460 (2014b)(Figure 12B). The tomographic image shows another deeper anomaly in the lower mantle that
461 requires a second rupture at the top of the pile in response to the pull of the slab diving into the lower
462 mantle (Figure 12C). At 39 ° S, the image of Pesicek et al. (2012) does not necessarily show this second
463 break up.

464
465 Numerical modeling shows that the way the slab deforms in depth depends strongly on the far-field
466 boundary conditions i.e. on the individual values of the subducting and overriding plate velocities (Gibert
467 et al., 2012; Cerpa et al., 2015). Two different styles of subduction are obtained once the subducting plate
468 reaches the 660 km discontinuity. If the overriding plate moves toward the trench or not, the slab
469 respectively lies forwards (case 1) or backwards (case 2) on the 660 km discontinuity (Figure 13). At the
470 first order, the South America plate always shifted to the west (i.e. to the trench) since the Atlantic
471 opening (e.g. Setton et al., 2012). But the absolute subduction velocity of the Nazca plate had always been
472 greater (e.g. Pardo-Casas & Molnar, 1987; Müller et al., 2018). This ratio of subducting and overriding

473 plate velocities is compatible with a folding of the slab above the 650 km mantle discontinuity as explored
474 by Gibert et al. (2012). And when folding occurs, the dip of the shallow slab changes.

475 Transient shallowing and steepening of the subducting slab has exerted an important influence on
476 orogenic patterns (e.g. Ramos et al., 2002, 2014; Haschke et al., 2002, 2006; Kay et al., 2006; Kay & Coira,
477 2009; Ramos & Folguera, 2009; Chen et al., 2019) and might force the evolution of basins. Indeed,
478 numerical modeling studies showed that the state of stress of the overriding plate is directly linked to the
479 absolute velocity of the upper plate and the dynamic of the lithospheric mantle but also to the dip of the
480 slab: upper plate shortening when the angle of the slab shallows, and extension when it steepens (Gibert
481 et al., 2012; Cerpa et al, 2014). Thus a cyclic stress regime in the overriding plate due to slab folding in
482 depth can be achieved with constant boundary conditions. Topography is also linked to the slab dip angle:
483 when the slab has a shallow dip angle, the upper plate shortens and the topography is positive. In turn,
484 when the slab dip angle steepens, the upper plate undergoes extension or less shortening and the
485 topography becomes negative. Numerical modeling predicts for the far-field plate kinematics setting of
486 the study area that these cycles will span about 20 Ma, depending of the mantle viscosity (Gibert et al.,
487 2012 ; Cerpa et al., 2014; 2015) with alternating pulses of compression, of lesser compression or tension
488 and episodes of regional uplift .

489 The seismic tomography shows also a vertical offset of about 200 km between both segments of the slab
490 where the first rupture of our scheme occurred (Figure 11 and 12; Pesicek et al., 2012). This break-off
491 might cause the basins to invert throughout an upward rebound of the remaining slab (Haschke et al.,
492 2006; Ramos et al., 2014). The authors do not yet agree on values of sinking rate of slabs in the mantle.
493 But the interval of proposed values is narrow, comprised between 10 +/- 2 mm/yr (Sigloch & Mihalynuk,
494 2017) and 13 +/- 3 mm/yr (Butterworth et al., 2014). The distance between the two segments of the slab
495 (i.e. 200 km) could yield a proxy of the onset of the slab break-off. We obtain here a value of 20 Ma
496 compatible with the timing of basin aggradation.

497
498 Focal-mechanism solutions of intermediate depth and deep earthquakes under the Japan Sea and the East
499 Asian margin (Zhao et al., 2009) show that the Pacific slab is under a compressional-stress regime in the
500 depth range of 200 to 600 km. Such a stress regime in the slab might be caused by the slab meeting strong
501 resistance at the 660-km discontinuity. In the same way, the asthenosphere under East China would be
502 both hot and wet, being associated with the deep dehydration of a stagnant Pacific slab (Ichiki et al.,

503 2006). The velocity field in the fluid also changes during fold development (Cerpa et al., 2014). The
504 convective circulation process in the upper mantle above the stagnant slab and the deep dehydration
505 process of the slab would cause upwellings of hot and wet asthenospheric materials, leading to the
506 formation of lithospheric attenuation as well as intraplate volcanoes (Zhao, 2012). This fits in the study
507 area observations by Folguera et al. (2018) who modeled the elastic thickness (T_e) of the study area.
508 Showing the coincidence between lowest values of T_e and emplacements of Plio-Quaternary magmatism,
509 they speculated that heating would have weakened crustal rigidity. However, T_e quickly increases toward
510 the foreland and reaches its maximum in the North Patagonian massif and its continuation to the north in
511 the Neuquén platform area where the lithosphere thickens (Tašárová, 2007).

512

513 **Conclusion**

514 The Collón Curá basin is one of these intramountainous basins of the Mio-Pliocene foothills of the
515 Patagonian Andes. Growing within the wedgetop depozone of a wider Andean foreland basin, sediments
516 accumulate above the active orogenic thrust wedge. Contrarily to other basins where accommodation is
517 achieved by their subsidence, that of these intramontane basins is by the dynamics of the tectonic barrier
518 which limits them (e.g. Hilley and Strecker, 2005). So the tectonic control is crucial for their development.
519 Former studies focused on the surface mapping and logging of the formations in order to obtain a
520 satisfactory stratigraphic frame. This must now be anchored on an absolute timing by multiplying
521 absolute dating of the filling. This effort must be made in order to overcome apparent contradictions rose
522 by the extrapolation of local data (e.g. Franzese et al., 2018).

523 Another important shortcoming concerns the subsurface data due to its lack of industrial potential. So
524 understanding of its articulation with the Paleogene history of the area remains unclear.

525

526 If tectonics plays a determining role in the evolution of these basins, it seemed important to us to
527 apprehend it in parallel with that of its neighbors. And it is striking to note that filling of these basins
528 occurred around 18 Ma. This filling answered to a regional event that authors called the Quechua phase.
529 However this episode did not correspond in the study area to a kinematic reorganization in terms of rates
530 or orientation of the South America and Nazca plates (Figures 9 and 10). The kinematics would not
531 explain to the first order this compressive episode.

532 In parallel to this, seismic tomography recently imaged anomalies of rapid velocities in the mantle that we
533 interpret as the relics of ancient slabs (Pesicek et al., 2012). It shows slab segments laying above the 660
534 km-depth mantle discontinuity and slab folding as those obtained in analogic and numerical models (e.g.
535 Guillaume et al., 2009; Gibert et al, 2012; Cerpa et al., 2014; Cerpa et al., 2015). This observation seems
536 important to us because mechanically, the slab controls the transfer of stress and strain between this
537 mantle discontinuity and the surface. Thus the state of stress of the overriding plate and topography too
538 link directly with the dip of the slab. An important result of this interpretation is that a cyclic stress regime
539 in the overriding plate can be achieved with constant boundary conditions. Thus the dynamics of
540 subduction, independently of its boundary conditions, imposes on the surface a cyclicity which will be
541 potentially inscribed in the sedimentary record.

542

543 If these basins are initiated at the same time, their excavation spreads itself over time. As a first
544 approximation, this results from the efficiency of the surface processes which, by reconnecting the basin
545 to its foreland, condemn it to excavation. This efficiency is determined by many parameters such as the
546 size of catchments, the slope of the flows, the lithology of the grounds which are specific to a given basin
547 and explains this spreading. But the development of slab folding, as it deposits on the 660 km depth
548 boundary, periodically flatten the slab with a strong impact on the state of stress and topography. Upper
549 plate shortening and uplift when the angle of the slab shallows, extension or lesser shortening and
550 subsidence when it steepens (e.g. Gibert et al., 2012; Cerpa et al, 2014). The balance between local uplift
551 (fault reactivation along the tectonic dam) and regional uplift (dynamic topography) through episodes of
552 higher shortening, will also interfere with surface processes. The evolution of these basins should also be
553 apprehended by the link to their close foreland that will generate or not space to accommodation. So a
554 quantification of the regional vertical displacements is required to constrain well the dynamics of these
555 basins.

556 Located in the hinterland of a volcanic arc, the combination of preserved landforms and abundant
557 intercalated volcanic ashes may resolve the timing of filling and excavation, tectonic activity, and
558 geomorphic evolution necessary to indentify a forcing of the internal dynamics of subduction on these
559 depozones.

560

- 561
562 Barrio, C., Carlini, A.A. and Goin, F.J., 1989. Litogenesis y antigüedad de la F. Chichinales de Paso Cordova
563 (Rio Negro, Argentina), *Actas 4° Congreso Argentino de Paleontología y Bioestratigrafía*, 4, 149–156.
564
- 565 Bechis, F. and Cristallini, E. O., 2005. Tectonic evolution of northern Niriuhau basin, northwestern Patagonia,
566 Argentina, 6th International Symposium on Andean Geodynamics (ISAG), Barcelona, 103-106.
567
- 568 Bechis, F., Encinas, A., Concheyro, A., Litvak, V., Aguirre-Urreta, B. and Ramos, V. 2014. New age constraints
569 for the Cenozoic marine transgressions of northwestern Patagonia, Argentina (41-43 S): Paleogeographic
570 and tectonics implications. *Journal of South American Earth Sciences*, 52, 72-93,
571 doi: 10.1016/j.jsames.2014.02.003.
572
- 573 Bilmes, A., D'Elia, L., Franzese, J., Veiga, G., Hernández, M., 2013. Miocene block uplift and basin formation
574 in the Patagonian foreland: The Gastre Basin, Argentina. *Tectonophysics*, 601, 98–111
575
- 576 Bilmes, A., D'Elia, L., Veiga, G.D., Franzese, J.R., 2014. Intermontane infill in the patagonian broken foreland:
577 Neogene evolution of the gastre Basin. *Revista de la Asociacion Geologica Argentina*, 71- 3, 311-330.
578
- 579 Branellec, M., Callot, J.P., Nivière, B., Ringenbach, J.C., 2015. The fracture network, a proxy for mesoscale
580 deformation: Constraints on layer parallel shortening history from the Malargüe fold and thrust belt,
581 Argentina. *Tectonics*, 34- 4, 623-647.
582
- 583 Branellec, M., Nivière, B., Callot, J. P., Ringenbach, J. C., 2016. Mechanisms of basin contraction and
584 reactivation in the basement-involved Malargue fold-and-thrust belt, Central Andes (34–36° S).
585 *Geological Magazine*, 153 (5-6), 926-944, doi: 10.1017/S0016756816000315.
586
- 587 Butterworth, N.P., Talsma, A.S., Müller, R.D., Seton, M., Bunge, H.P., Schuberth, B.S.A., Shephard, G.E.,
588 Heine, C., 2014. Geological, tomographic, kinematic and geodynamic constraints on the dynamics of
589 sinking slabs. *Journal of Geodynamics*, 73, 1–13, doi: 10.1016/j.jog.2013.10.006 .
590
- 591 Cazau, L., Mancini, D., Cangini, J., Spalletti, L., 1989. Cuenca de Niriuhau. In: Chebli, G., Spalletti, L. (Eds.),
592 Cuenca Sedimentarias Argentinas, Serie Correlación Geológica, vol. 6. Universidad Nacional de
593 Tucumán, pp. 299–318.
594
- 595 Cazau, L., Cortiñas, J., Reinante, S., Asensio, M., Bechis, F., Apreda, D., 2005. Cuenca de Niriuhau. In: Chebli,
596 G., Cortiñas, J.S., Spalletti, L., Legarreta, L., Vallejo, E.L. (Eds.), *Frontera Exploratoria de la Argentina*,
597 IV Congreso de Exploración y Desarrollo de Hidrocarburos, pp. 251–273.
598
- 599 Cerpa, N.G., Hassani, R., Gerbault, M., Prévost, J.-H., 2014. A fictitious domain method for lithosphere-
600 asthenosphere interaction: Application to periodic slab folding in the upper mantle. *Geochem. Geophys.*
601 *Geosyst.*, 15, 1852–1877, doi:10.1002/2014GC005241.
602
- 603 Cerpa, N.G., Araya, R., Gerbault, M., Hassani R., 2015. Relationship between slab dip and topography
604 segmentation in an oblique subduction zone: Insights from numerical modelling. *Geophys. Res. Lett.*, 42,
605 5786–5795, doi:10.1002/2015GL064047.
606
- 607 Chen, Y.-W., Wu, J. and Suppe, J., 2019. Southward propagation of Nazca subduction along the Andes,
608 *Nature*, 565, 441–447.
609
- 610 Cobbold, P.R., Rossello, E.A., 2003. Aptian to recent compressional deformation, foothills of the Neuquén
611 Basin, Argentina. *Mar. Petrol. Geol.*, 20, 429–443.
612
- 613 Costa, C., Cisneros, H., Salvarredi, J., Gallucci, A., 2006. La neotectónica del margen oriental del bloque de San
614 Rafael: Nuevas consideraciones. *Asociación Geológica Argentina, Serie D: Publicación Especial*, 6, 33–
615 40.
616
- 617 Cucchi, R., Leanza, H., 2005. Hoja Geológica 3972-IV Junín de los Andes, provincia del Neuquén. *Servicio*
618 *Geológico Minero Nacional. Boletín* 357, 1-102.

619
620 Curtis, G.H., 1966. The problem of contamination in obtaining accurate dates of young geologic rocks, In
621 Shaeffer, O. A., & Zahringer, J., eds., Potassium-Argon dating, Springer-Verlag, New York, p.151-162.
622
623 Deino, A. L., Tauxe, L., Monaghan, M. And Drake, R., 1990. Single-crystal $^{40}\text{Ar}/^{39}\text{Ar}$ ages and the litho- and
624 paleomagnetic stratigraphies of the Negorora Formation, Kenya Rift, *Journal of Geology*, 98, 567-587.
625
626 D'Elia, L., Muravchik, M., Franzese, J.R., Lopez, L., 2012. Tectonostratigraphic analysis of the Late Triassic-
627 Early Jurassic syn-rift sequence of the Neuquén Basin in the Sanico depocentre, Neuquén Province,
628 Argentina. *Andean Geol.*, 39, 133–157.
629
630 Dessanti, R.N., 1972. Andes Patagónicos Septentrionales. In: *Geología Regional Argentina* (Ed. by A.F.
631 Leanza), pp. 655–688. Academia Nacional de Ciencias, Córdoba.
632
633 Escosteguy, L., Franchi, M., 2010. Estratigrafía de la región de Chapelco, Provincia del Neuquén. *Revista de la*
634 *Asociación Geológica Argentina*, 66, 418–429.
635
636 Flint, R.F., Fidalgo, F., 1968. Drift glacial al este de los Andes entre Bariloche y Esquel. *Inst. Nac. Geol. y Min*
637 *Bol.*, 119, 1–14.
638
639 Folguera, A., Zapata, T., Ramos, V.A., 2006. Late Cenozoic Extension and the evolution of the Neuquén Andes.
640 In: Kay, S.M., Ramos, V.A. (Eds.), Late Cretaceous to Recent Magmatism and Tectonism of the
641 Southern Andean Margin at the Latitude of the Neuquen Basin (36–39°S). Geological Society of
642 America, Special Paper, vol. 407, pp. 267–285.
643
644 Folguera, A., Gianni, G., Encinas, A., Alvarez, O., Orts, D., Echaurren, A., Litvak, V. D., Navarrete, C.,
645 Sellés, D., Tobal, J., Ramos, M., Fennell, L., Giménez, M., Martínez, P., Ruiz, F. and Iannelli, S., 2018.
646 Neogene Growth of the Patagonian Andes. In: Folguera A. et al. (eds) *The Evolution of the Chilean-*
647 *Argentinean Andes*. Springer Earth System Sciences. Springer, Cham
648
649 Franzese, J.R., D'Elia, L., Bilmes, A., Muravchik, M. & Hernández, M., 2011. Superimposition of Oligo-
650 Miocene extensional and contractional basins in the North Patagonian Andean retroarc: The Aluminé
651 basin, Neuquén, Argentina. *Andean Geology*, 38- 2, 319-334.
652
653 Franzese, J.R., D'Elia, L., Bilmes, A., Bucher, J., García, M., López, M., Muravchik, M. & Hernández, M., 2018.
654 Evolution of a patagonian Miocene intermontane basin and its relationship with the Andean foreland:
655 Tectono-stratigraphic evidences from the Catán Lil Basin, Argentina. *Journal of South American Earth*
656 *Sciences*, 86, 162-175.
657
658 Galli, C.A., 1954. Acerca de una nueva interpretación de las Formaciones Rético-liásicas de la Patagonia
659 septentrional. *Revista de la Asociación Geológica Argentina*, 8, 220–235.
660
661 Galli, C.A., 1969. Descripción geológica de la Hoja 38c, Piedra del Aguila, Province Del Neuquén y Río Negro.
662 *Dir. Nac. Geol. Min. Bol.*, 111, 1–65.
663
664 García Morabito, E., Ramos, V.A., 2012. Andean evolution of the aluminé fold and thrust belt, northern
665 Patagonian Andes (38°30'–40°30'S). *J. South Am. Earth Sci.* 38, 13–30.
666
667 García Morabito, E.G., Götze, H.J., Ramos, V.A., 2011. Tertiary tectonics of the Patagonian Andes retro-arc
668 area between 38°15' and 40°S latitude. *Tectonophysics*, 499, 1–21.
669
670 Giacosa, R., Heredia, N., 1999. La cuenca de antepaís terciaria asociada a la faja plegada y corrida de los Andes
671 Patagónicos entre los 41° y 42° SO de Argentina. In: Busquets, P., Colombo, F., Perez-Estaun, A.,
672 Rodríguez Fernández, R., (Eds.), *Geología de los Andes Centrales Argentino-Chilenos. Acta Geológica*
673 *Hispanica* 32 (1–2), 103–111.
674
675 Giacosa, R., Heredia, N., Cesari, O., Zubia, M., 2001. Hoja geológica 4172-IV, San Carlos de Bariloche
676 (provincias de Río Negro y Neuquén). Instituto de Geología y Recursos Minerales, *Servicio Geológico*
677 *Minero Argentino. Boletín* 279, 67p.
678

679 Gibert, G., Gerbault, M., Hassani, R., Tric, E., 2012. Dependency of slab geometry on absolute velocities and
680 conditions for cyclicity: Insights from numerical modelling. *Geophys. J. Int.*, 189-2, 747–760,
681 doi:10.1111/j.1365-246X.2012.05426.x.
682
683 González Bonorino, F., 1973. Geología del área entre San Carlos de Bariloche y Llao-Llao, vol. 16. Fundación
684 Bariloche, Publicación, 53p.
685
686 González Bonorino, F., González Bonorino, G., 1978. Geología de la región de San Carlos de Bariloche.
687 *Asociación Geológica Argentina, Revista* 33-3, 175–210.
688
689 González Díaz, E.F., Nullo, F., 1980. Cordillera Neuquina. Segundo Simposio de Geología Regional Argentina,
690 *Acad. Nac. Cienc.*, 2, 1099–1147.
691
692 González Díaz, E.F., Riggi, J.C., Fauqué, L., 1986. Formación Caleufu (Nov. Nom): reinterpretación de las
693 Formaciones Rio Negro y Alicura, en el área de Collón Cura, sur del Neuquén. *Asociación Geológica*
694 *Argentina, Revista* XLI, 1–2, 81–105.
695
696 González Díaz, E.F., Osters, H.A., Riggi, J.C., Fauqué, L., 1990. Una propuesta temporal acerca del Miembro
697 Limay Chico (ex “Rionegrense”) de la Formación Caleufu, en el valle del río Collón Cura y adyacencias
698 (SE del Neuquén). 11° Congreso Geológico Argentino (San Juan), 2, 243–246.
699
700 Gracia, R., 1958. Informe geológico de las Cartas Paso Flores y Traful. Secret. Ejerc. Direc. Gral. Ing., Buenos
701 Aires.
702
703 Grimaldi, G. O. and Dorobek, S. L., 2011. Fault framework and kinematic evolution of inversion structures:
704 Natural examples from the Neuquén Basin, Argentina. *AAPG Bulletin*, 95, 1, 27–60.
705
706 Groeber, P., 1951. La Alta Cordillera entre las latitudes 34° y 29°30', *Revista del Instituto Nacional de*
707 *Investigaciones de las Ciencias Naturales, Museo Argentino de Ciencias Naturales “Bernardino*
708 *Rivadavia”, Buenos Aires, Argentina, 1-5, 235–352.*
709
710 Guillaume, B., Martinod, J., Espurt, N., 2009. Variations of slab dip and overriding plate tectonics during
711 subduction: Insights from analogue modelling, *Tectonophysics*, 463(14), 167-174,
712 doi:10.1016/j.tecto.2008.09.043.
713
714 Gurnis, M., Yang, T., Cannon, J., Turner, M., Williams, S., Flament, N., Müller, R. D., 2018. Global tectonic
715 reconstructions with continuously deforming and evolving rigid plates, in: *Computers & Geosciences*,
716 116, 32-41. doi:10.1016/j.cageo.2018.04.007.
717
718 Haschke, M., Scheuber, E., Gunther, A., Reutter, K.-J., 2002. Evolutionary cycles during the Andean orogeny:
719 repeated slab breakoff and flat subduction? *Terra Nova*, 14, 49–55.
720
721 Haschke, M., Günther, A., Melnick, D., Echtler, H., Reutter, K.-J., Scheuber, E., Oncken, O., 2006. Central and
722 Southern Andean tectonic evolution inferred from arc magmatism, in *The Andes*, Springer, Berlin, pp.
723 337–353.
724
725 Heuret, A., Funiciello, F., Faccenna, C., Lallemand, S., 2007. Plate kinematics, slab shape and back-arc stress: a
726 comparison between laboratory models and current subduction zones. *Earth Planet. Sci. Lett.* 256 (3),
727 473e483.
728
729 Hilley, G.E. and Strecker, M.R., 2005. Processes of oscillatory basin filling and excavation in a tectonically
730 active orogen: Quebrada del Toro Basin, NW Argentina, *Geol. Soc. Am. Bull.*, 117, 887–901.
731
732 Hosseini, K., Matthews, K. J., Sigloch, K., Shephard, G. E., Domeier, M. and Tsekhmistrenko, M., 2018.
733 Submachine: Web-Based tools for exploring seismic tomography and other models of Earth’s deep
734 interior. *Geochemistry, Geophysics, Geosystems*, 19, doi:10.1029/2018GC007431.
735
736 Hugo, C.A., Leanza, H.A., 2001. Hoja Geológica 3669-IV, General Roca. Provincia del Neuquén. Instituto de
737 Geología y Recursos Minerales, Servicio Geológico Minero Argentino 308, 70.
738

739 Huyghe, D., Bonnel, C., Nivière, B., Fasentieux, B., Hervouët, Y., 2015a. Neogene tectonostratigraphic history
740 of the southern Neuquén basin (39°-40°30'S, Argentina): implications for foreland basin evolution. *Basin*
741 *Res.*, 27 (5), 613-635. doi: 10.1111/bre.12091
742

743 Huyghe, D., Nivière, B., Bonnel, C., 2015b. Geomorphologic evidence for Plio-Quaternary shortening in the
744 southern Neuquén basin (40°S, Argentina). *Terra Nova*, 27-6, 426-432.
745

746 Ichiki, M., Baba, K., Obayashi, M., Utada H., 2006. Water content and geotherm in the upper mantle above the
747 stagnant slab: Interpretation of electrical conductivity and seismic P-wave velocity models. *Phys. Earth*
748 *Planet. Inter.*, 155, 1-15.
749

750 Jordan, T.E., 1995. Retroarc Foreland and Related Basins. In: Tectonics of Sedimentary Basins (Ed. by C.J.
751 Busby, R.V. Ingersoll), Blackwell Science, Oxford., pp. 331-362.
752

753 Kay, S.M., Burns, M., Copeland, P., 2006. Upper Cretaceous to Holocene Magmatism over the Neuquén basin:
754 Evidence for transient shallowing of the subduction zone under the Neuquén Andes (36° S to 38° S
755 latitude). In: Kay SM, Ramos VA (eds) Late Cretaceous to Recent magmatism and tectonism of the
756 Southern Andean margin at the latitude of the Neuquén basin (36–39° S). *Geological Society of America,*
757 *Special Paper*, 407, 19-60
758

759 Kay, S.M., Coira, B.L., 2009. Shallowing and steepening subduction zones, continental lithospheric loss,
760 magmatism, and crustal flow under the Central Andean Altiplano-Puna Plateau. In: Kay S.M., Ramos
761 V.A., Dickinson W.R. (eds) Backbone of the Americas: Shallow Subduction, Plateau Uplift, and Ridge
762 and Terrane Collision. *Geol. Soc. Am. Memoirs*, Boulder, 204, 229-259
763

764 Lagorio, S., Montenegro, T., Massafiero, G., Vattuone, M.E., 1998. Edad y geoquímica de las ignimbritas de
765 Alumíné, provincia del Neuquén, Argentina. In Congreso Latinoamericano de Geología, Buenos Aires,
766 10-2, 321-325.
767

768 Leanza, H.A., Hugo, C.A., Herrero, J.C., Donnari, E., Pucci, J.C., 1997. Hoja Geológica 3969-III, Picun Leufu.
769 Instituto de Geología y Recursos Minerales, *Servicio Geológico Minero Argentino: Boletín* 218, 135.
770

771 Leanza, H.A., Hugo, C.A. (2001) Hoja Geológica 3969-I, Zapala. Instituto de Geología y Recursos Minerales,
772 Servicio Geológico Minero Argentino: Boletín 275, 135pp.
773

774 Li, C., van der Hilst, R. D., Engdahl, E. R. and Burdick, S., 2008. A new global model for P wave speed
775 variations in Earth's mantle, *Geochem. Geophys. Geosyst.*, 9, Q05018, doi:10.1029/2007GC001806.
776

777 Lo Bello, P., Féraud, G., Hall, C. M., York, D., Lavina, P., and Bernat, M., 1987. ⁴⁰Ar/³⁹Ar step-heating and laser
778 fusion dating of a Quaternary pumice from Neschert, Massif Central, France: The defeat of xenocrystic
779 contamination, *Chemical Geology*, 66, p. 61-71.
780

781 Lorito, S., Romano, F., Atzori, S., Tong, X., Avallone, A., McCloskey, J., Cocco, M., Boschi, E., Piatanesi, A.,
782 2011. Limited overlap between the seismic gap and coseismic slip of the great 2010 Chile earthquake,
783 *Nature Geosci.*, 4(3), 173–177.
784

785 Mancini, D., Serna, M., 1989. Evaluación petrolera de la Cuenca de Ñirihuau. Sudoeste de Argentina. 1
786 Congreso Nacional de Exploración de Hidrocarburos (Argentina). *Actas* 2, 739-762.
787

788 Margirier, A., Audin, L., Robert, X., Pêcher, A. and Schwartz, S., 2017. Stress field evolution above the
789 Peruvian flat-slab (cordillera Blanca, northern Peru). *Journal of South American Earth Sciences*, 77, 58-
790 69.
791

792 Marshall, L.G., Pascual, R., Curtis, G.H., Drake, R.E., 1977. South american geochronology: radiometric time
793 scale for middle to late tertiary mammal-bearing horizons in patagonia. *Science*, 195, 1325-8.
794 <https://doi.org/10.1126/science.195.4284.1325>
795

796 Mazzoni, M., Benvenuto, A., 1990. Radiometric ages of Tertiary ignimbrites and the Collón Curá Formation
797 northwestern Patagonia. In: XI Congreso Geológico Argentino, San Juan, pp 87–90.
798

- 799 Mazzoni, M.M., Rapela, C.W., 1991. Características químicas e isotópicas de ignimbritas Miocenas. Andes
800 Patagónicas septentrionales (SVZ), Argentina. Congreso Geológico Chileno, 6, 125–128.
801
- 802 McDougall, I., Brown, F.H., Cerling, T.E. and Hillhouse, J.W., 1992. A reappraisal of the geomagnetic polarity
803 time scale to 4 MA using data from the Turkana Basin, East Africa, *Geophysical Research Letters*, 19, 23,
804 2349-2352, doi : 10.1029/92GL02714.
805
- 806 Messenger, G., Nivière, B., Martinod, J., Lacan, P., Xavier, J.-P., 2010. Geomorphic evidence for Plio-Quaternary
807 compression in the Andean foothills of the southern Neuquén Basin, Argentina. *Tectonics*, 29, 1–18.
808 doi:10.1029/2009TC002609.
809
- 810 Meijer, P.Th. and Wortel, M.J.R., 1992. The dynamics of motion of the South American
811 Plate. *Journal of Geophysical Research: Solid Earth*, 97(B8), 11915–1193.
812
- 813 Meyer, B., Saltus, R. and Chulliat, A., 2017. EMAG2: Earth Magnetic Anomaly Grid (2-arc-
814 minute resolution) Version 3. National Centers for Environmental Information,
815 NOAA. Model. doi:10.7289/V5H70CVX
816
- 817 Mosquera, A., Ramos, V.A., 2006. Intraplate deformation in the Neuquén Embayment. In: Evolution of an
818 Andean margin: A Tectonic and Magmatic View from the Andes to the Neuquén Basin (35°-39°S lat)
819 (Ed. by S.M. Kay & V.A. Ramos), *Geol. S. Am. S.*, 407, 97–123.
820
- 821 Müller, R.D., Cannon, J., Qin, X., Watson, R.J., Gurnis, M., Williams, S., et al. 2018. GPlates: Building a virtual
822 Earth through deep time, in: *Geochemistry, Geophysics, Geosystems*, 19, 2243-2261.
823 doi:10.1029/2018GC007584.
824
- 825 Naipauer M, García Morabito E, Marques JC, Tunik V, Rojas Vera E, Vujovich GI, Pimentel MP and Ramos
826 VA, 2012. Intraplate Late Jurassic deformation and exhumation in western central Argentina: Constraints
827 from surface data and U-Pb detrital zircon ages. *Tectonophysics*, 524-525 (1), 59-75.
828
- 829 Nullo, F., 1979. Descripción geológica de la Hoja 39c, Paso Flores, provincias de Río Negro y Neuquén.
830 *Servicio Geológico Nacional, Boletín*, 167, 73p.
831
- 832 Orts, D., Folguera, A., Encinas, A., Ramos, M., Tobal, J., Ramos, V.A., 2012. Tectonic development of the
833 North Patagonian Andes and their related Miocene foreland basin (41°30'–43° S). *Tectonics* 31- TC3012.
834 <https://doi.org/10.1029/2011TC003084>
835
- 836 Pardo-Casas, F., Molnar, P., 1987. Relative motion of the Nazca (Farallón) and South American plates since
837 Late Cretaceous time. *Tectonics*, 6, 233-248
838
- 839 Paredes, J.M., Giacosa, R.E., Heredia, N., 2009. Sedimentary evolution of Neogene continental deposits
840 (Ñirihuau Formation) along the Ñirihuau River, North Patagonian Andes of Argentina. *Journal of South
841 American Earth Sciences*, 28-1, 74-88. DOI: 10.1016/j.jsames.2009.01.002
842
- 843 Pascual, R., Odreman Rivas, O., 1971. Evolución de las comunidades de los vertebrados del Terciario
844 Argentino. Los aspectos paleozoogeográficos y paleoclimáticos relacionados. *Ameghiniana*, 8, 372–412.
845
- 846 Pascual, R.P., Bondesio, M.G., Vucetich, G., Scillato Ya~Ne, G., Bond, M. & Tonni, E.P., 1984. Vertebrados
847 fósiles cenozoicos. Relatorio 9º Congreso Geológico Argentino, 2, 439–461.
848
- 849 Pesicek, J.D., Engdahl, E.R., Thurber, C.H., Deshon, H.R., Lange, D., 2012. Mantle subducting slab structure in
850 the region of the 2010 M8.8 Maule earthquake (30-40°S), Chile. *Geophysical Journal International*,
851 191- 1, 317-324.
852
- 853 Rabassa, J., 1975. Geología de la región de Pilcaniyeu-Comallo, Provincia de Río Negro, Argentina. Publicación
854 Fundación Bariloche, Departamento Recursos Naturales y Energéticos, San Carlos de Bariloche. Vol. 17,
855 129 pp.
856
- 857 Rabassa, J., 1978. Estratigrafía de la región de Pilcaniyeu-Comallo, Provincia de Río Negro. In: 7 Congreso

858 Geológico Argentino, Buenos Aires, Actas I: 731-746.
859
860 Ramos, V., Cortés, J., 1984. Estructura e interpretación tectónica. In: Ramos, V. (Ed.), Geología y Recursos
861 Naturales de la Provincia de Río Negro, 1- 12, 317–346.
862
863 Ramos, V.A., Folguera, A., 2009. Andean flat-slab subduction through time. *Geol. Soc. Lond. Special Publ.*,
864 327-1, 31-54, doi:10.1144/SP327.3.
865
866 Ramos, V.A., Cristallini, E., Pérez, D.J., 2002. The Pampean flat-slab of the Central Andes. *J. S. Am. Earth Sci.*,
867 15, 59-78.
868
869 Ramos, V.A., Litvak, V., Folguera, A., Spagnuolo, M., 2014a. An Andean tectonic cycle: from crustal
870 thickening to extension in a thin crust (34°-37°SL). *Geosci. Front.*, 5, 351–367.
871
872 Ramos, M.E., Folguera, A., Fennel, L., Giménez, M., Litvak, V.D., Dzierma, Y., Ramos, V.A., 2014b. Tectonic
873 evolution of the North Patagonian Andes from field and gravity data (39-40°S). *J. S. Am. Earth Sci.*, 51,
874 59–75.
875
876 Ramos, M., Tobal, J., Sagripanti, L., Folguera, A., Orts, D., Giménez, M., Ramos, V., 2015. The North
877 Patagonian orogenic front and foreland evolution: Ñirihuau-Ñorquinco Depocenter (-42° S). *J. South Am.*
878 *Earth. Sci.*, 64, 467–485.
879
880 Rapela, C.W., Spalletti, L.A., Merodio, J., 1983. Evolucion magmatica y geotectonica de la “Serie Andesítica”
881 andina en la Cordillera Norpatagonica. *Rev. Asoc. Geol. Argent.*, 38, 469-484.
882
883 Rapela, C., Spalletti, L.A., Merodio, J., Aragón, E., 1988. Temporal evolution and spatial variations of early
884 Tertiary volcanism in the Patagonian Andes. (40 S–42° 30' S). *J. South Am. Earth. Sci.*, 1-1, 75–88.
885
886 Renne, P., R., 2000. K-Ar and ⁴⁰Ar/³⁹Ar Dating, In J., S. Noller, J., M. Sowers & W. R. Lettis (Eds.),
887 Quaternary Geochronology: Methods and Applications, Volume 4, (pp. 77-100), Washington DC,
888 American Geophysical Union.
889
890 Renne, P.R., Deckart, K., Ernesto, M., Féraud, G., Piccirillo, E.M., 1996. Age of the Ponta Grossa dike swarm
891 (Brazil), and implications to Paraná flood volcanism, *Earth and Planetary Science Letters*, 144 (1-2), 199-
892 211.
893
894 Renne, P.R., Walter, R., Verosub, K., Sweitzer, M., and Aronson, J., 1993. New data from Hadar (Ethiopia)
895 support orbitally tuned time scale to 3.3 MA, *Geophysical Research Letters*, 20 (11), 1067-1070.
896
897 Rojas Vera, E.A., Selles, D., Folguera, A., Gimenez, M., Ruíz, F., Orts, D., Zamora Valcarce, G., Martínez, P.,
898 Bechis, F., Ramos, V.A., 2014. The origin of the Loncopué trough in the retroarc of the Southern Central
899 Andes from field, geophysical and geochemical data. *Tectonophysics*, 637, 1–19
900
901 Rolleri, E., Dellap_E, D.A. & Mance~Nido, M.O., 1984. Relaciones estratigraphicas y correlación de las
902 Formaciones Pichi Picún Leufú y Collón Cura (Miembro Naupa Huen) aflorantes en el curso inferior y
903 medio del cañadón Michihuau, provincia de Río Negro. 9° Congreso Geológico, 1, 257–265.
904
905 Roth, S., 1899. Reconocimiento de la region andina de la Republica Argentina. Apuntes sobre la geologia y
906 paleontología de Rio Negro y Neuquén. *Revista Museo de La Plata*, 9, 141–197.
907
908 Roth, S., 1922. Investigaciones geológicas en la región norte de la Patagonia durante los años 1897 a 1899.
909 *Revista del Museo de La Plata*, 26, 333–392.
910
911 Ruff, L.J. and Kanamori, H., 1983. Seismic coupling and uncoupling at subduction zones, *Tectonophysics*, 99
912 (2-4), 9-117.
913
914 Sánchez, N., Coutand, I., Turienzo, M., Lebinson, F., Araujo, V. and Dimier, L., 2017. Middle Miocene to Early
915 Pliocene Contraction in the ChosMalal Fold-and-Thrust Belt (Neuquén Basin, Argentina): Insights From
916 Structural Analysis and ApatiteFission-Tracks Thermochronology, *Tectonics*, 36, 10, 1966-1987,
917 doi.org/10.1002/2017TC004516.

918
919 Schellart, W.P., 2008. Overriding plate shortening and extension above subduction zones: a parametric study to
920 explain formation of the Andes Mountains, *Geol. Soc. Am. Bull.*, 120 (11-12), 1441-1454.
921
922 Seton, M., Müller, R.D., Zahirovic, S., Gaina, C., Torsvik, T., Shephard, G., Talsma, A., Gurnis, M., Turner, M.,
923 Maus, S., and Chandler, M., 2012. Global continental and ocean basin reconstructions since 200 Ma:
924 *Earth- Science Reviews*, 113, 212-270, doi: 10.1016/j.earscirev.2012.03.002.
925
926 Sigloch, K., Mihalynuk, M.G., 2013. Intra-oceanic subduction shaped the assembly of Cordilleran North
927 America, *Nature*, 496- 7443, 50-56.
928
929 Sigloch, K., Mihalynuk, M.G., 2017. Mantle and geological evidence for a Late Jurassic–Cretaceous suture
930 spanning North America, *Geological Society of America Bulletin*, 129 (11-12), 1489-1520, doi:
931 10.1130/B31529.1
932
933 Spalletti, L.A., 1981. Facies sedimentarias de la Formación Ñirihuau en la región de San Carlos de Bariloche,
934 provincia de Río Negro. *Asociación Geológica Argentina Revista*, 36-3, 286–311.
935
936 Spalletti, L.A., Dalla Salda, L., 1996. A pull-apart volcanic related Tertiary Basin, an example from the
937 Patagonian Andes. *Journal of South American Earth Sciences*, 9 (1–4), 197–206.
938
939 Steinmann, G., Lissón, C.I., Sieberg, A., Stappenbeck, R., 1929. Geologie von Peru, Winter, Heidelberg,
940 Germany.
941
942 Tašárová, Z.A., 2007. Towards understanding the lithospheric structure of the southern Chilean subduction zone
943 (36° S-42° S) and its role in the gravity field. *Geophys. J. Int.*, 170, 995–1014. doi:
944 <https://doi.org/10.1111/j.1365-246X.2007.03466.x>
945
946 Turner, J.C.M., 1965. Estratigrafía de Aluminé y adyacencias, provincia de Neuquén. *Asociación Geológica*
947 *Argentina*, Revista 20-2, 153–184.
948
949 Turner, J.C.M., 1965. Estratigrafía de Aluminé y adyacencias. *Rev. Asoc. Geol. Argent.* 20, 153-164.
950
951 Turner, J.C.M., 1973. Descripción geológica de la Hoja 37 a-b, Junin de los Andes, provincia del Neuquén.
952 *Servicio Nacional Minero Geológico, Boletín*, Buenos Aires, 138, 86pp.
953
954 Vergani, G.D., Tankard, A.J., Belotti, H.J. and Welsink, H.J., 1995. Tectonic evolution and paleogeography of
955 the Neuquén Basin, Argentina. In: Petroleum Basins of South America (A.J. Tankard, R. Suarez, R.
956 Soruco and H.J. Welsink, eds). *AAPG Mem.*, 62, 383-402.
957
958 Volkheimer, W., 1964. Estratigrafía de la zona extraandina del Departamento de Cushman (Chubut) entre los
959 paralelos de 42° y 42°30' y los meridianos 70° y 71°. *Asociación Geológica Argentina, Revista* 19-2, 85–
960 107.
961
962 Yrigoyen, M.R., 1969. Problemas estratigráficos del terciario de Argentina. *Ameghiniana*, 6, 315–329.
963
964 Zhao, D., Tian, Y., Lei, J., Liu, L., Zheng, S., 2009. Seismic image and origin of the Changbai intraplate volcano
965 in East Asia: Role of big mantle wedge above the stagnant Pacific slab, *Phys. Earth Planet. Inter.*, 173,
966 197–206.
967
968 Zhao, D., 2012. Tomography and Dynamics of Western-Pacific Subduction Zones, *Monogr. Environ. Earth*
969 *Planets*, 1-1, 1–70.
970
971
972
973

973 FIGURE CAPTIONS

974

975 **Figure 1:** Neogene intra mountaine basins (yellow patches) of the North Patagonian foothill with main
976 structures above the shaded topography. Inset with location of Figure 1 in South America.

977

978 **Figure 2:** Geological map of the southern Neuquén basin with location of the Collón Curá basin (location
979 in Figure 1). Red dots are the sedimentary sections in Figure 3.

980

981 **Figure 3:** Sedimentary sections in the Collón Curá basin (from Huyghe et al., 2015a). Stars are the sampled
982 ignimbrites for dating ($^{40}\text{Ar}/^{39}\text{Ar}$ on biotite).

983

984 **Figure 4:** Synthesis of the ages of Cenozoic sedimentary formations in the southern part of the Neuquén
985 basin. Dating results are from: 1: Barrio et al. (1989), 2: Pascual et al. (1984), 3: Rolleri et al. (1984), 4:
986 Pascual and Odreman Rivas (1971), 5: Marshall et al. (1977), 6: Gonzalez Diaz and Nullo (1980), 7:
987 Rabassa (1975), 8: Mazzoni and Buenvenuto (1990), 9: Cazau et al. (1989), 10: Gonzalez Diaz et al. (1990),
988 11: Ramos et al. (2014b) and 12: this study. Biostratigraphic ages are in blue and radiometric ages are in
989 red.

990

991 **Figure 5:** $^{40}\text{Ar}/^{39}\text{Ar}$ age spectra for the two sampled ignimbrites at the outcropping base and at the top
992 of the Collón Curá Basin. Ar-11-15 (top) is concordant, Ar-11-30 (bottom) is discordant.

993

994 **Figure 6:** Paleogeographic sketch map of the Collón Curá Basin and foreland from early Miocene (bottom)
995 to Present (top).

996

997 **Figure 7:** Compilation of the ages of the sedimentary filling of the main intra montane basins between 38
998 and 41°S. Ages are from Roth (1922); González Bonorino (1973); Giacosa et al. (2001); Cazau et al. (2005)
999 and Paredes et al. (2009) for the Ñirihuau Basin; from Marshall et al. (1977); Rabassa (1978); Rapela et al.
1000 (1983); Mazzoni and Benvenuto (1990); Cucchi y Leanza (2005); Orts et al. (2012); Bilmes et al. (2013,
1001 2014); Ramos et al. (2014b, 2015); Rojas Vera et al. (2014) and Franzese et al. (2018) for the Catan Lil
1002 basin; Leanza & Hugo (2001) and Messenger et al. (2010) for the Agua Amarga Basin, and this study for the

1003 Collón Curá Basin. The bottom of the sedimentary infill does not outcrop in the Collón Curá Basin, so
1004 aggradation began before the dated ignimbrite Ar-11-30 (around 19 Ma). The light grey triangles show the
1005 uncertainty on onset of aggradation.

1006

1007 **Figure 8:** Oceanic spreading rates above the South Atlantic (dashed lines) and South Pacific (dotted lines)
1008 ridges at 37 and 40°S from Oligocene to Present (from Meyer et al., 2017).

1009

1010 **Figure 9:** Location of the South America plate with respect to the current geographical frame through time
1011 from Oligocene to Present. South America continuously moved to the northwest during this time interval
1012 (from Müller et al., 2018).

1013

1014 **Figure 10:** Convergence rates (red) and angle of convergence (violet) between the Nazca and South
1015 America plates from Oligocene to Present at the latitude of the Collón Curá basin (40°S; from Müller et al.,
1016 2018).

1017

1018 **Figure 11:** A) Seismic tomographic image of lithosphere and lower mantle at 37 and 39°S (from Pesicek
1019 et al., 2012). B) Analogical modeling of slab folding above the 660 km-depth mantle discontinuity (from
1020 Guillaume et al., 2009).

1021

1022 **Figure 12:** An interpretation of the seismic tomographic image by Pesicek et al. (2012). A) Stacking of slab
1023 folds above the 660 km-depth mantle discontinuity and its stagnation could force convective circulation
1024 process in the upper mantle and a deep dehydration process of the slab. The resulting upwellings of hot
1025 and wet asthenospheric materials could lead to lithospheric attenuation and intraplate volcanoes (Zhao,
1026 2012). B) First shallow slab break-off with upward rebound of the remaining slab (Haschke et al., 2006).
1027 This break-off might cause the basins to invert. C) Second deep slab break-off at the top of the slab fold
1028 stack with sinking in the lower mantle.

1029

1030 **Figure 13:** Four characteristic modes of subduction toward the ocean (mode 2b) or the continent (other
1031 modes) and implying folding of the oceanic slab (mode 1a and 2a) or not (mode 1b and 2b). The arrows
1032 show far-field absolute plates velocities (black arrows indicate trenchward motion). The symbol ⊗

1033 indicates that the velocity is zéro (from Gibert et al., 2012).

1034

1035

39°S

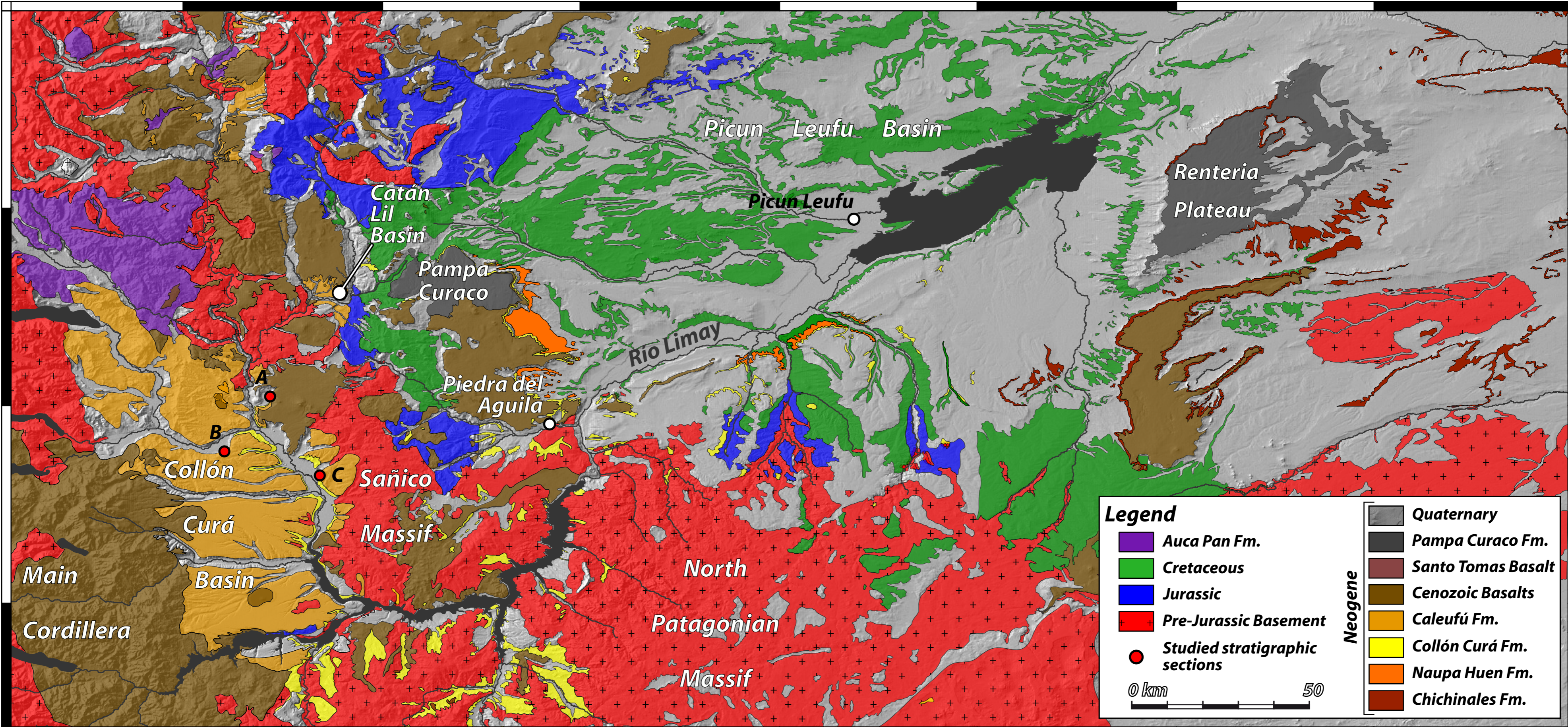
40°S

71°W















70°W

69°W

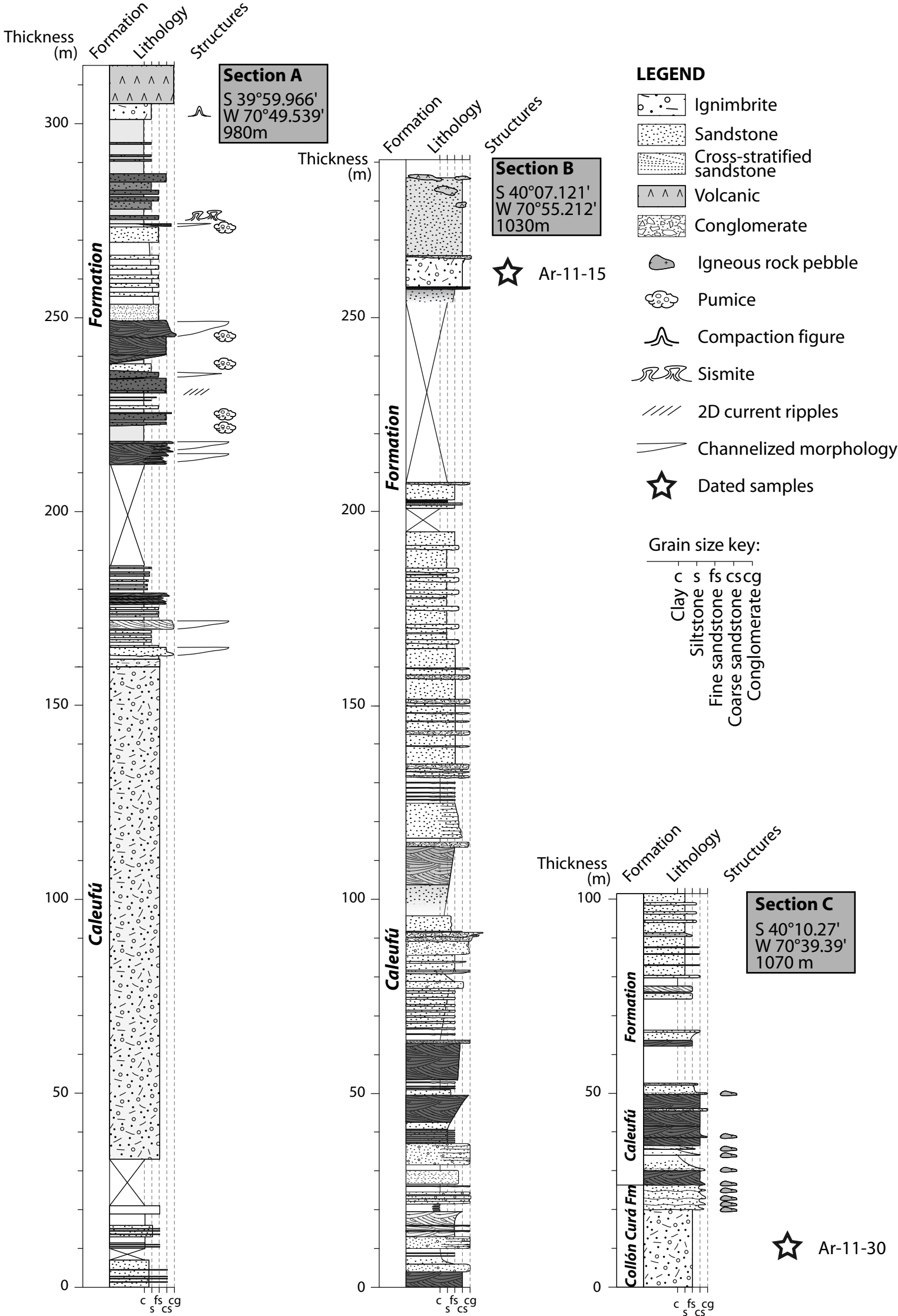
68°W

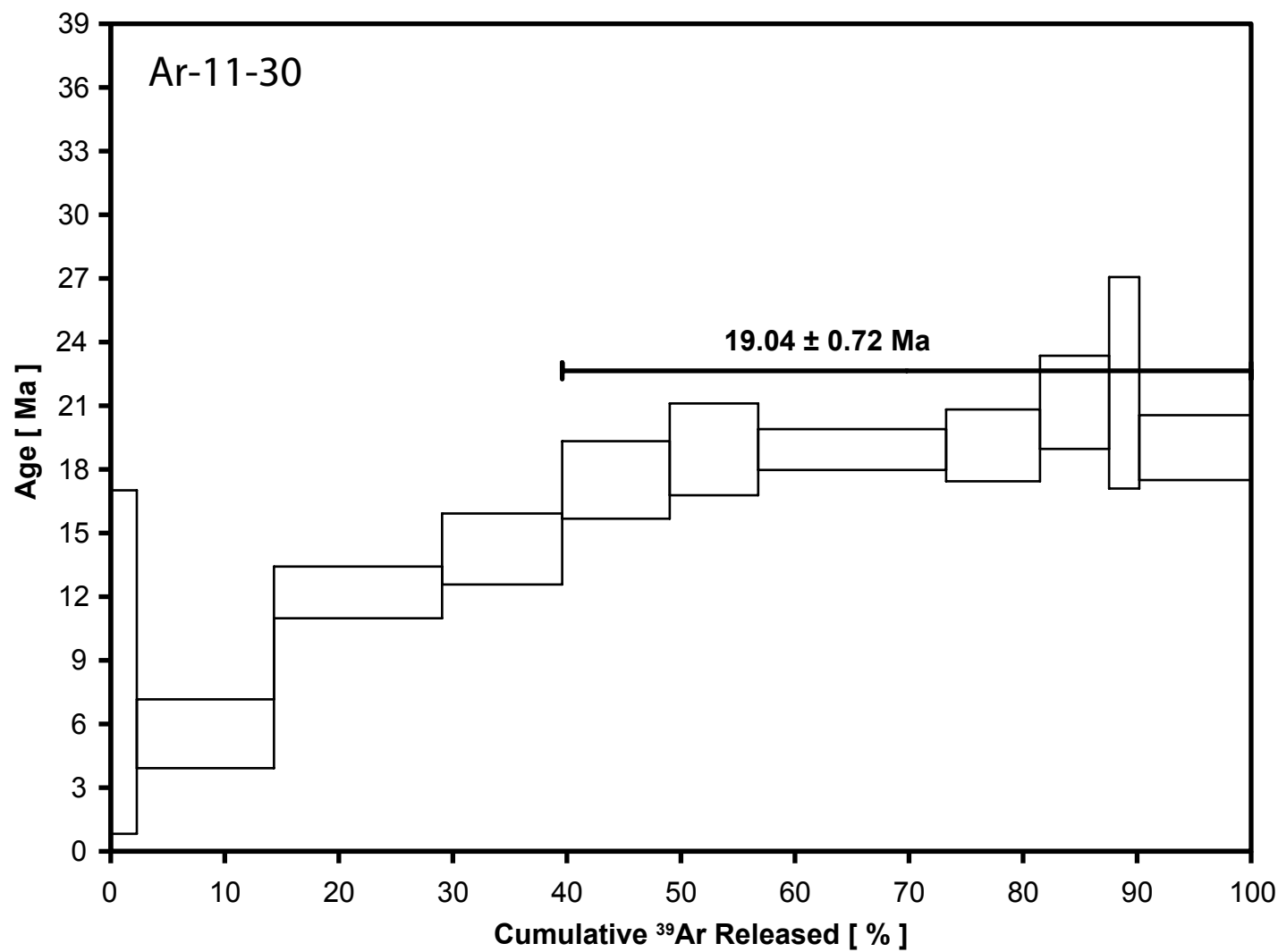
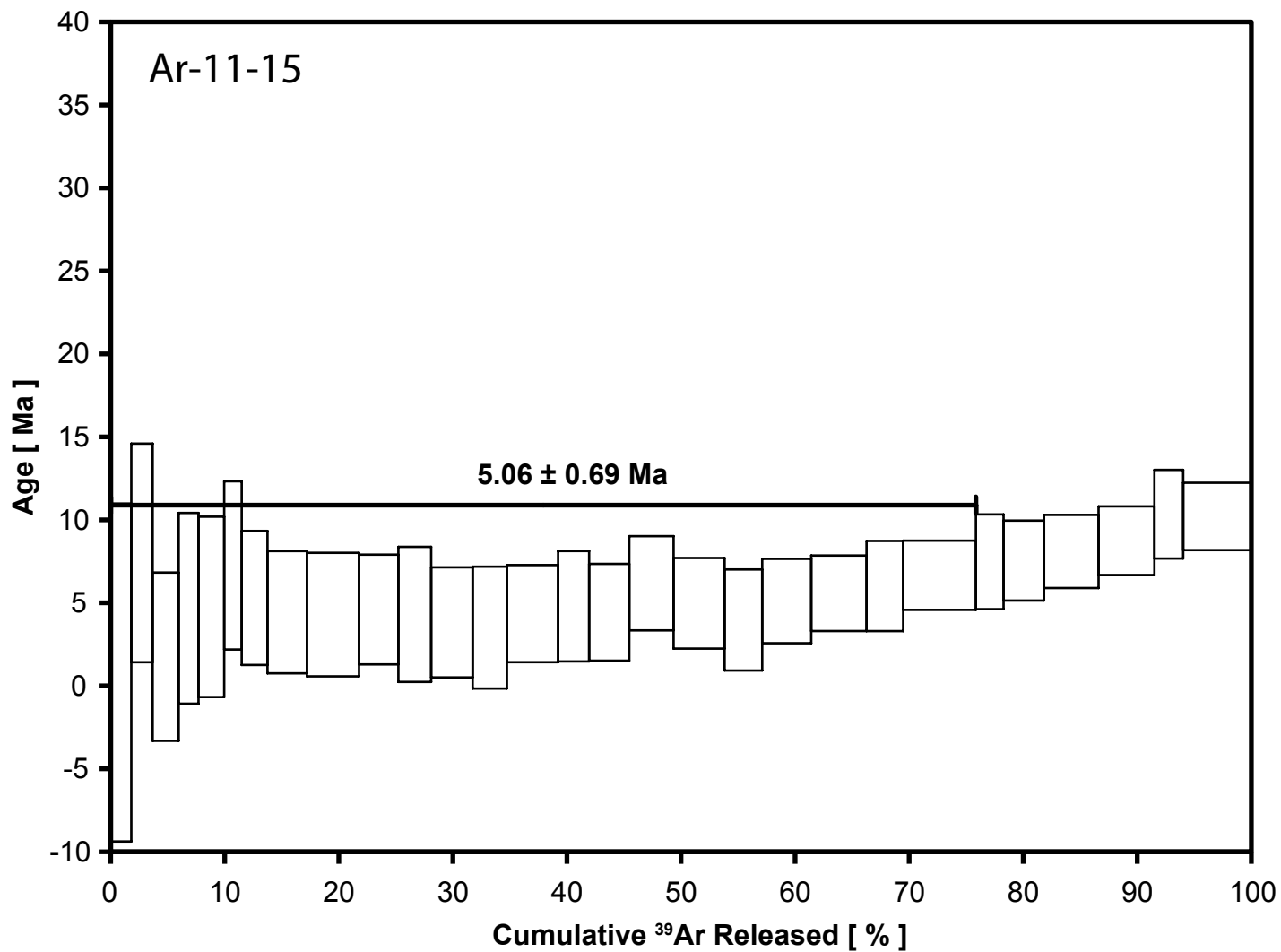


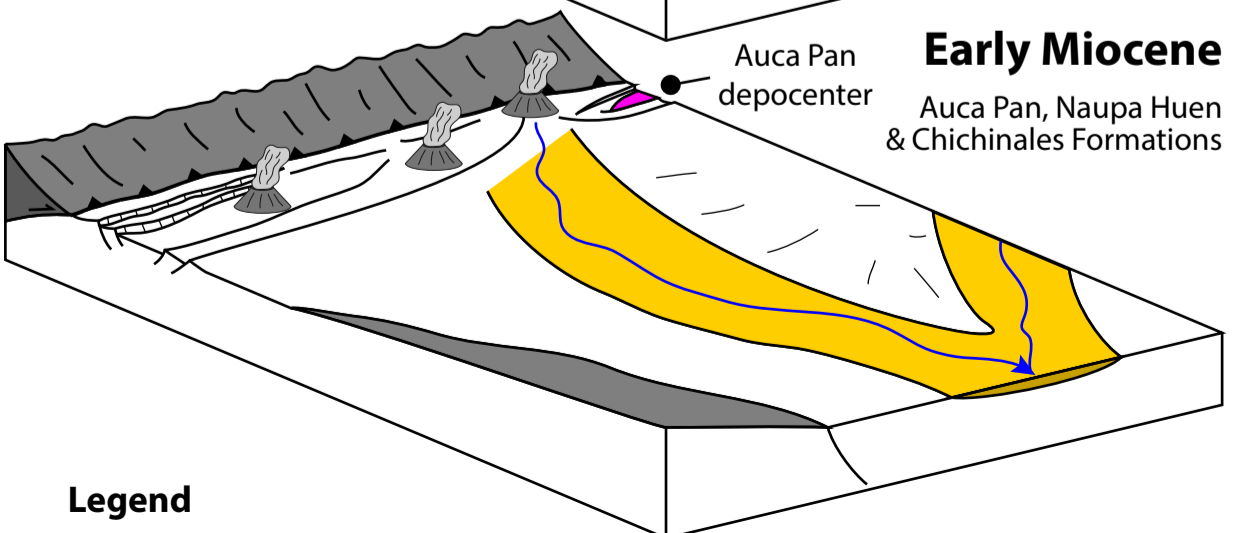
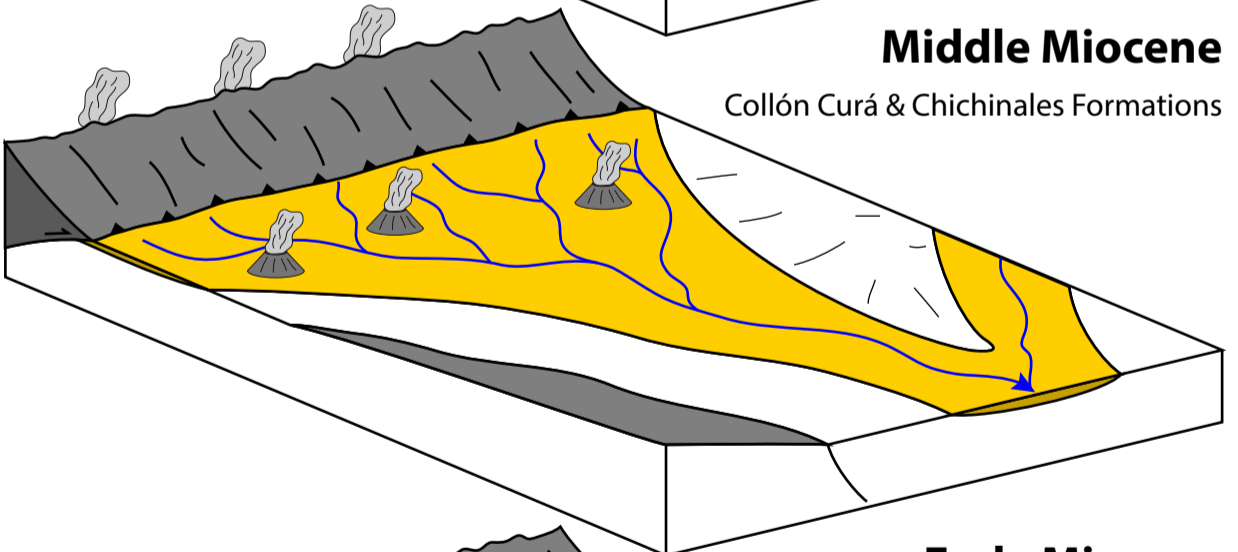
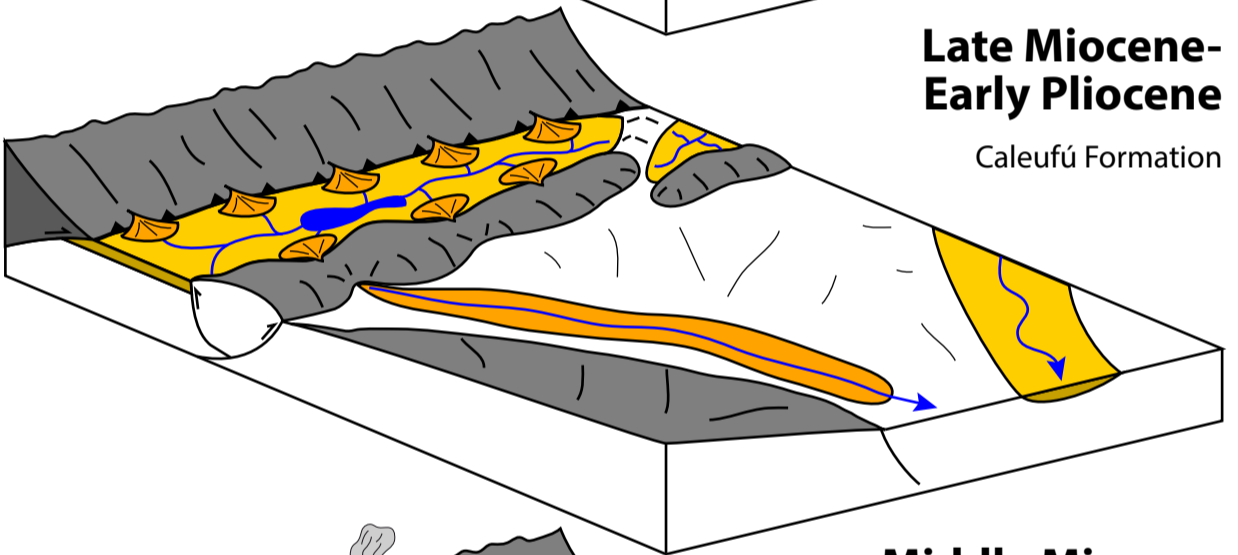
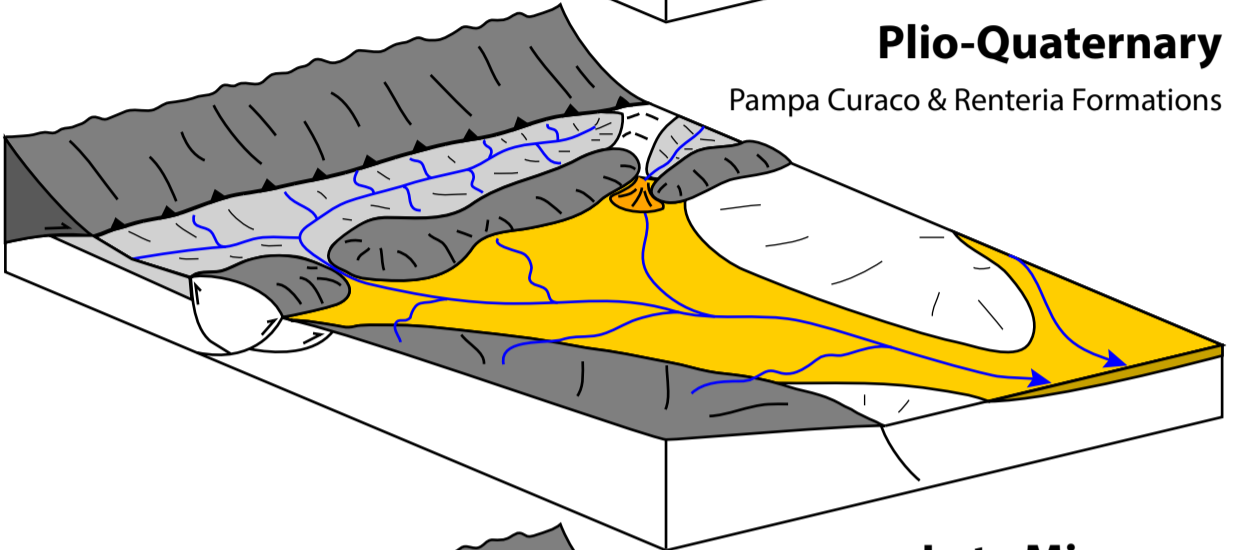
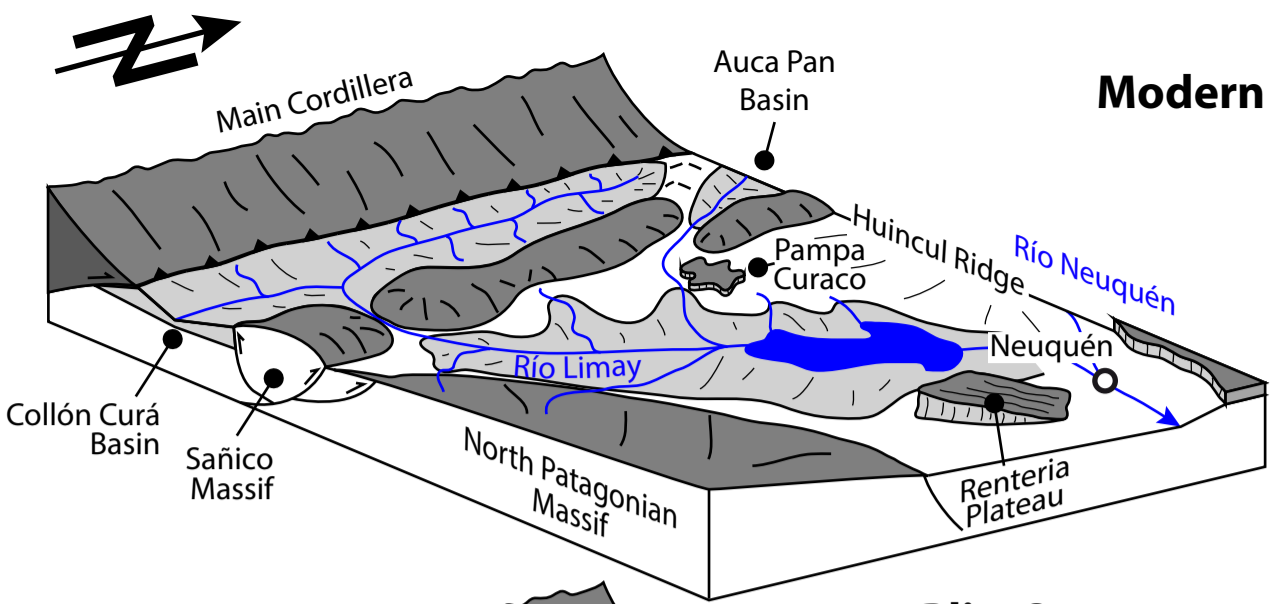
Legend

 Auca Pan Fm.	 Quaternary
 Cretaceous	 Pampa Curaco Fm.
 Jurassic	 Santo Tomas Basalt
 Pre-Jurassic Basement	 Cenozoic Basalts
 Studied stratigraphic sections	 Caleufú Fm.
	 Collón Curá Fm.
	 Naupa Huen Fm.
	 Chichinales Fm.

Neogene

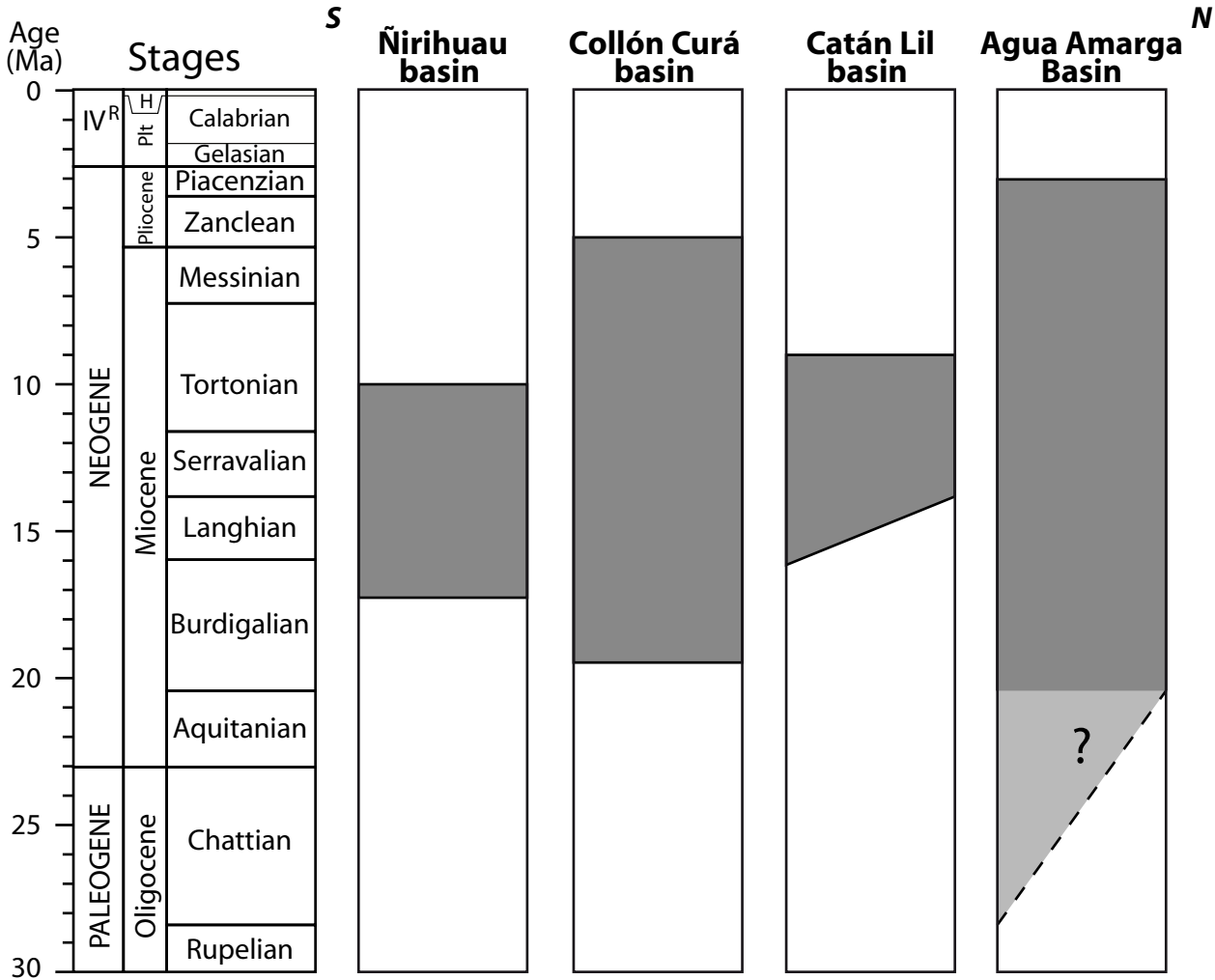


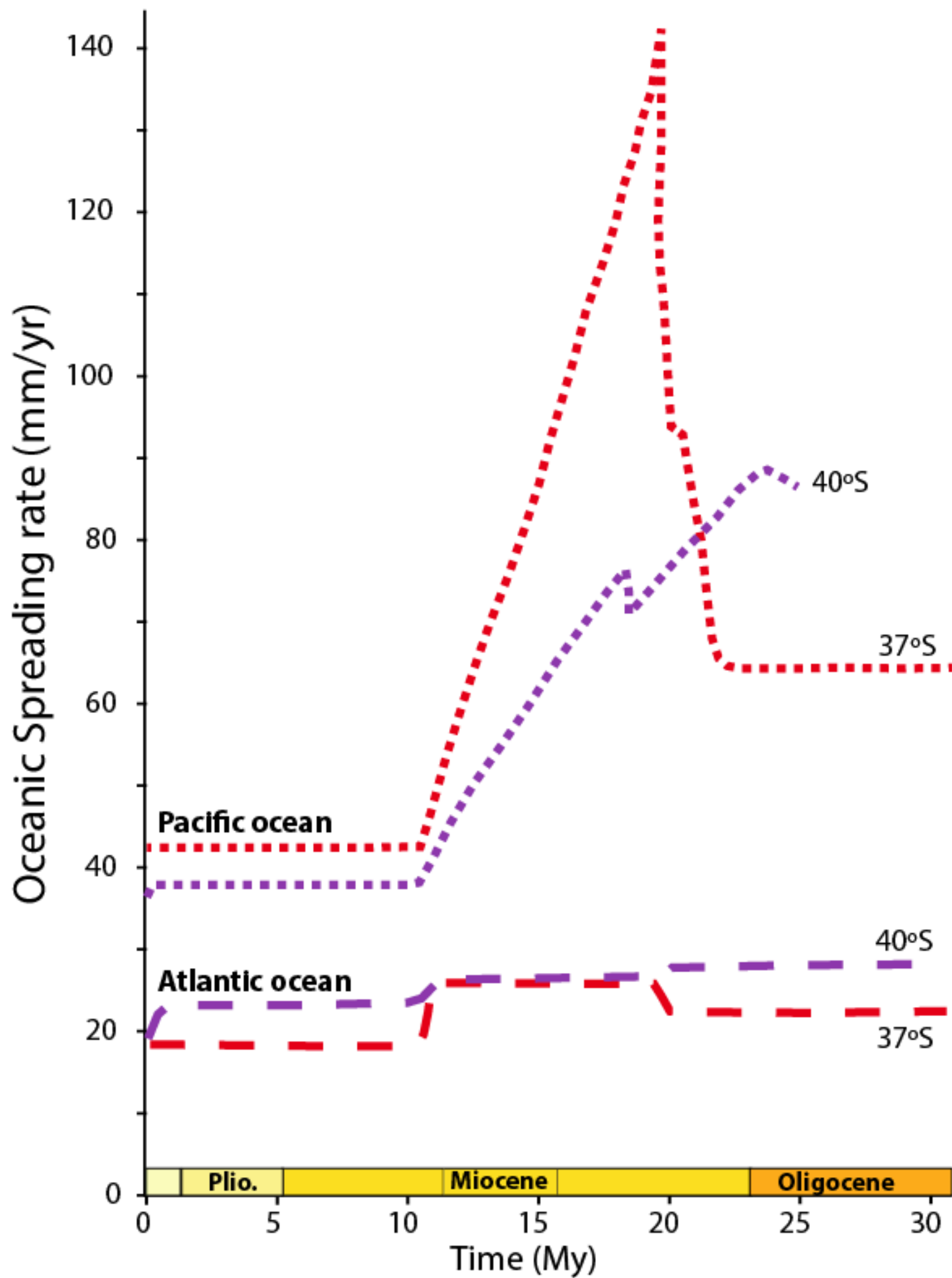


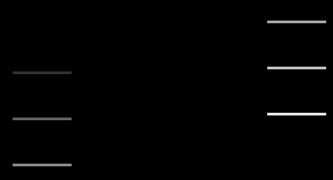
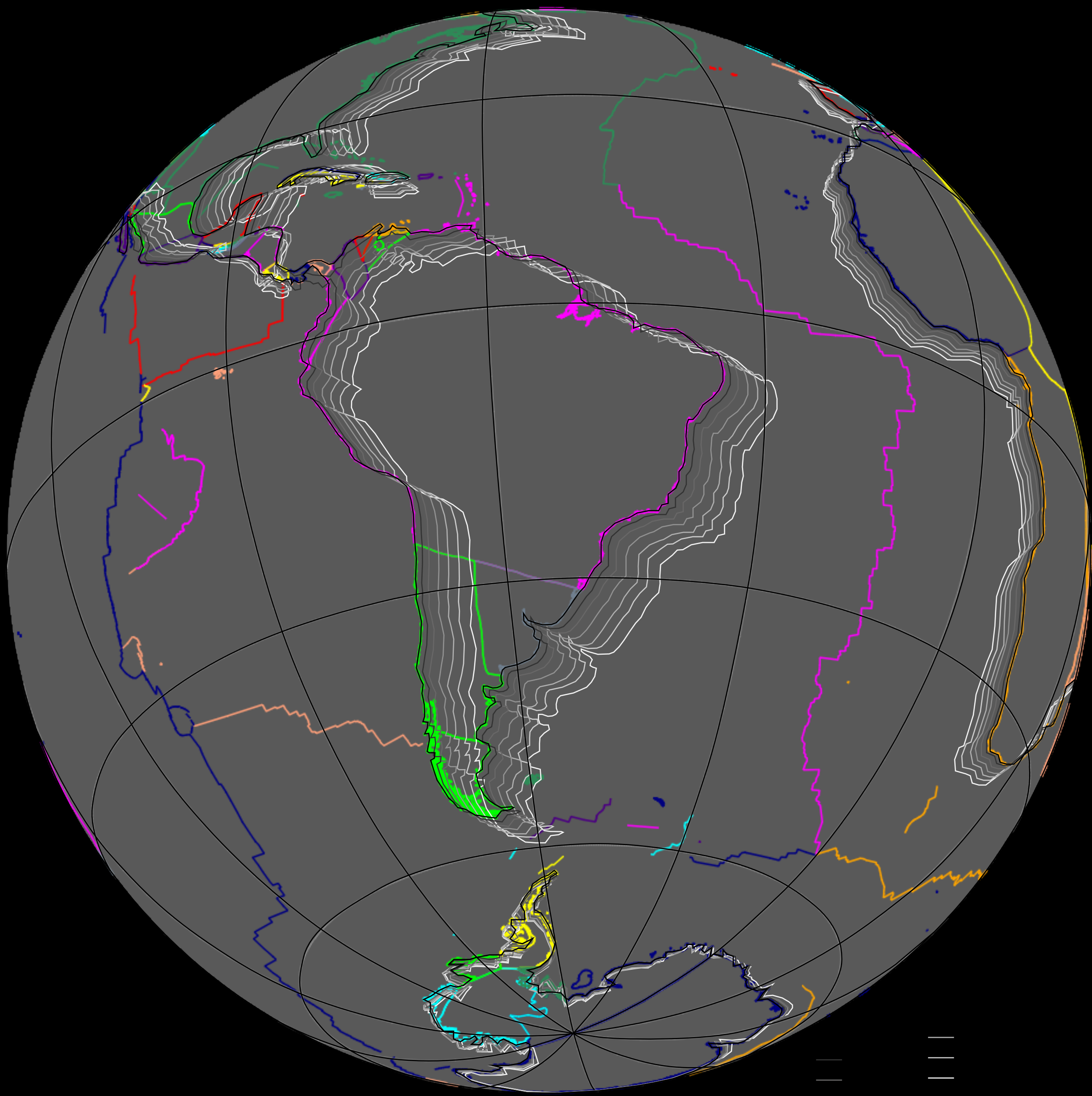


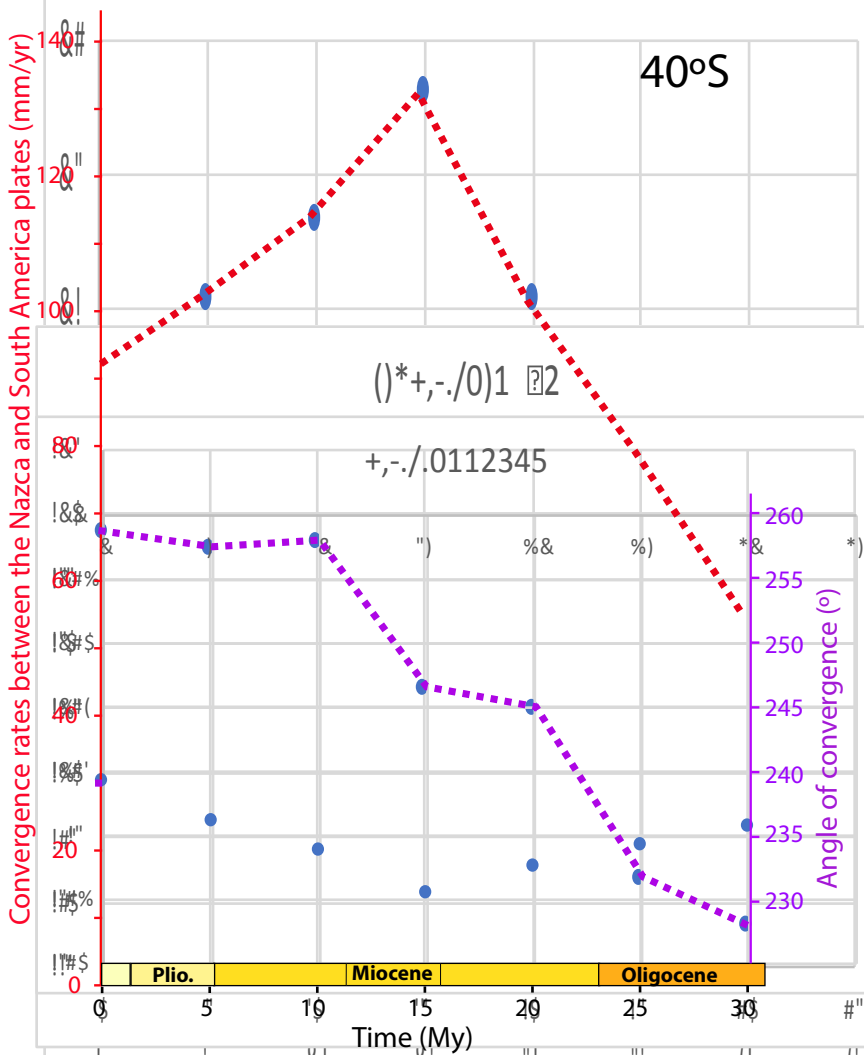
Legend

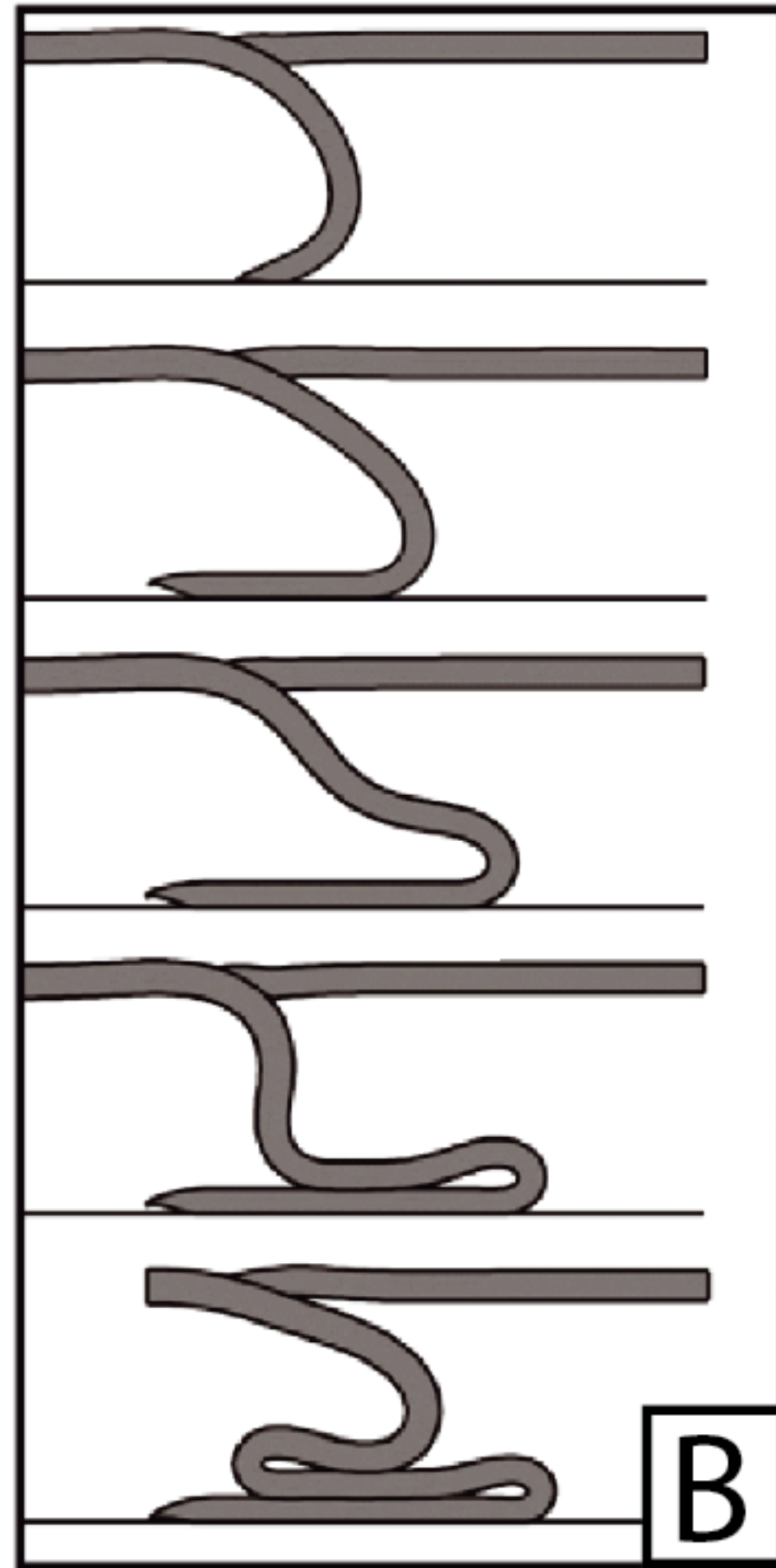
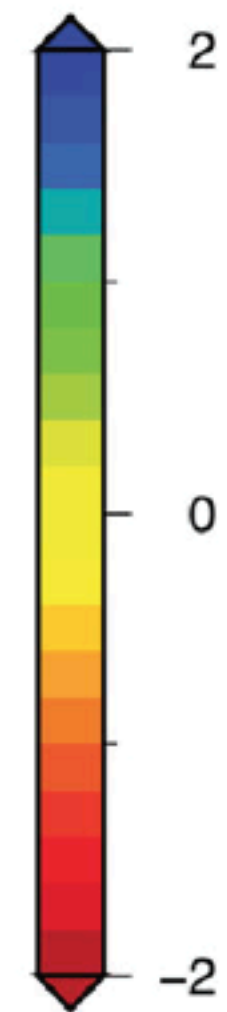
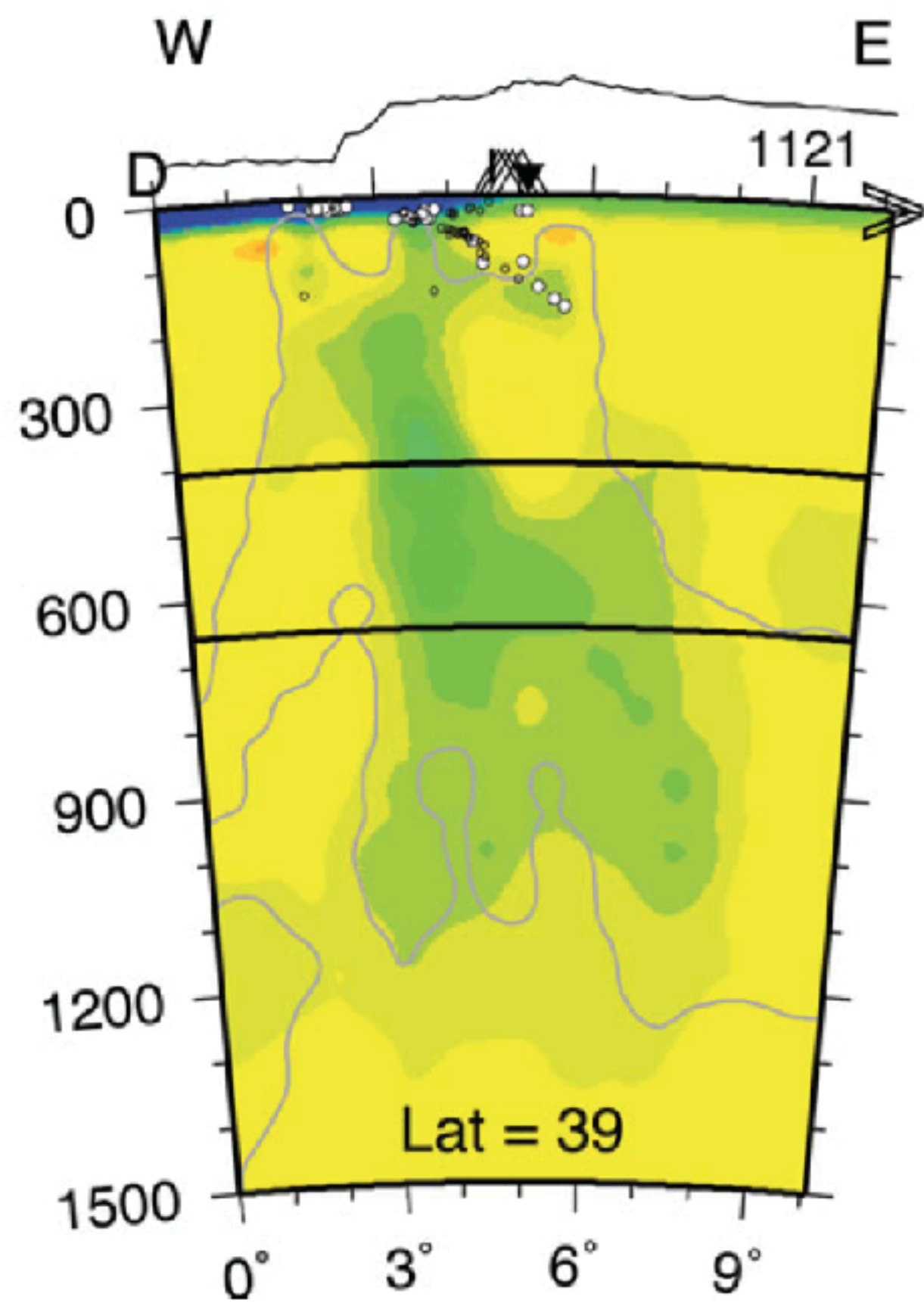
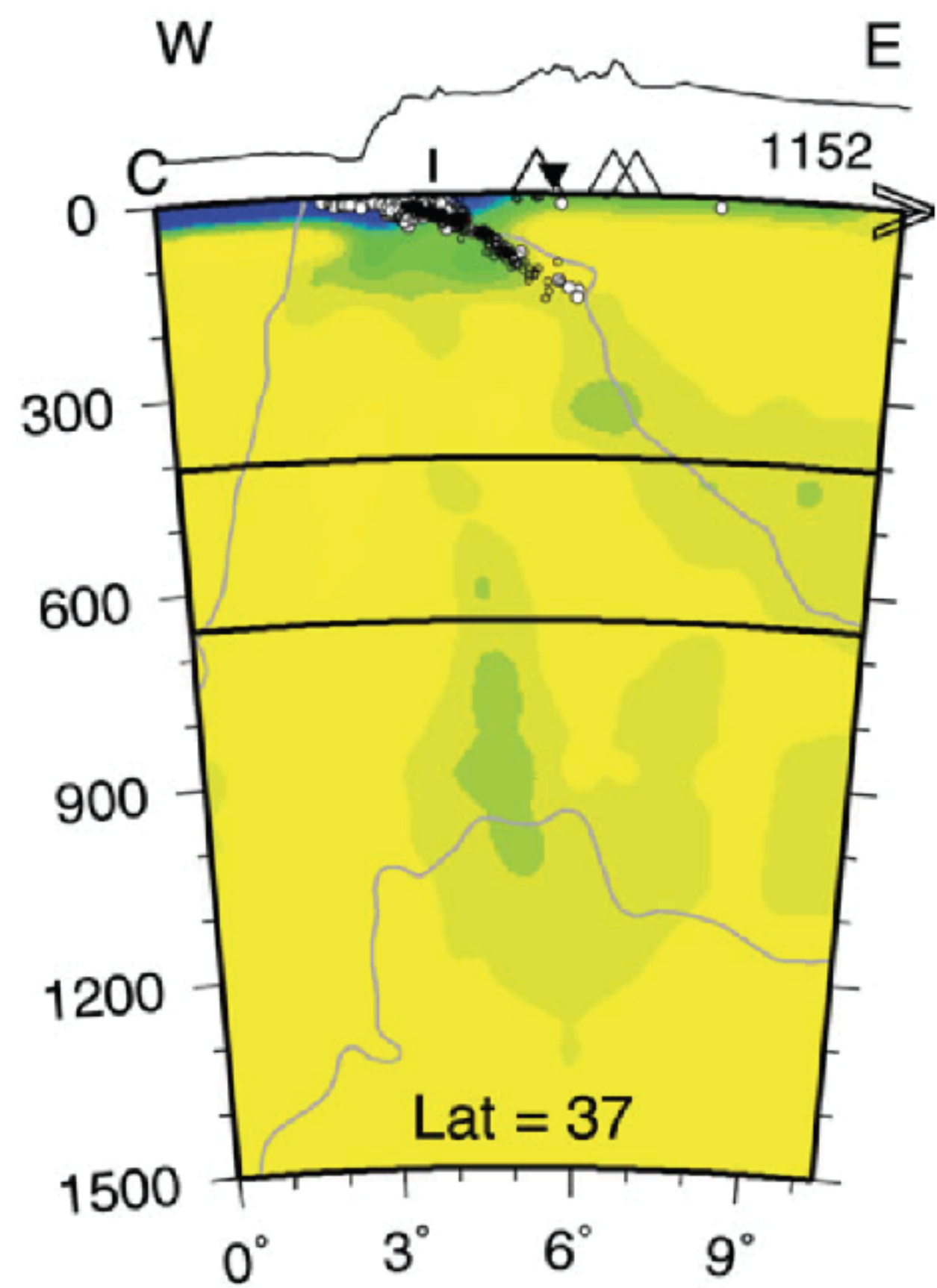
- Uplifted area
- Basin in erosion
- Fluvial environment
- Alluvial fan
- Auca Pan formation

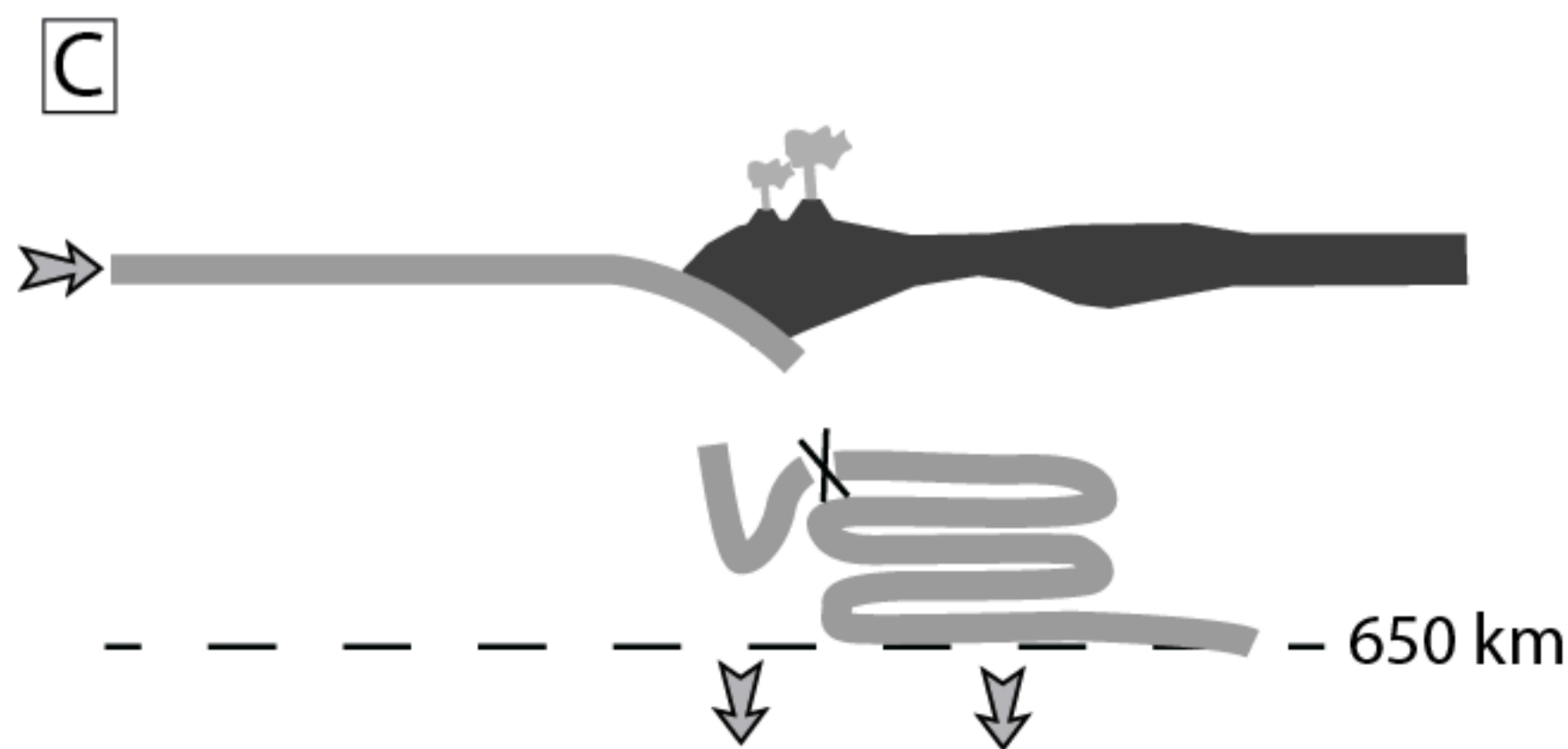
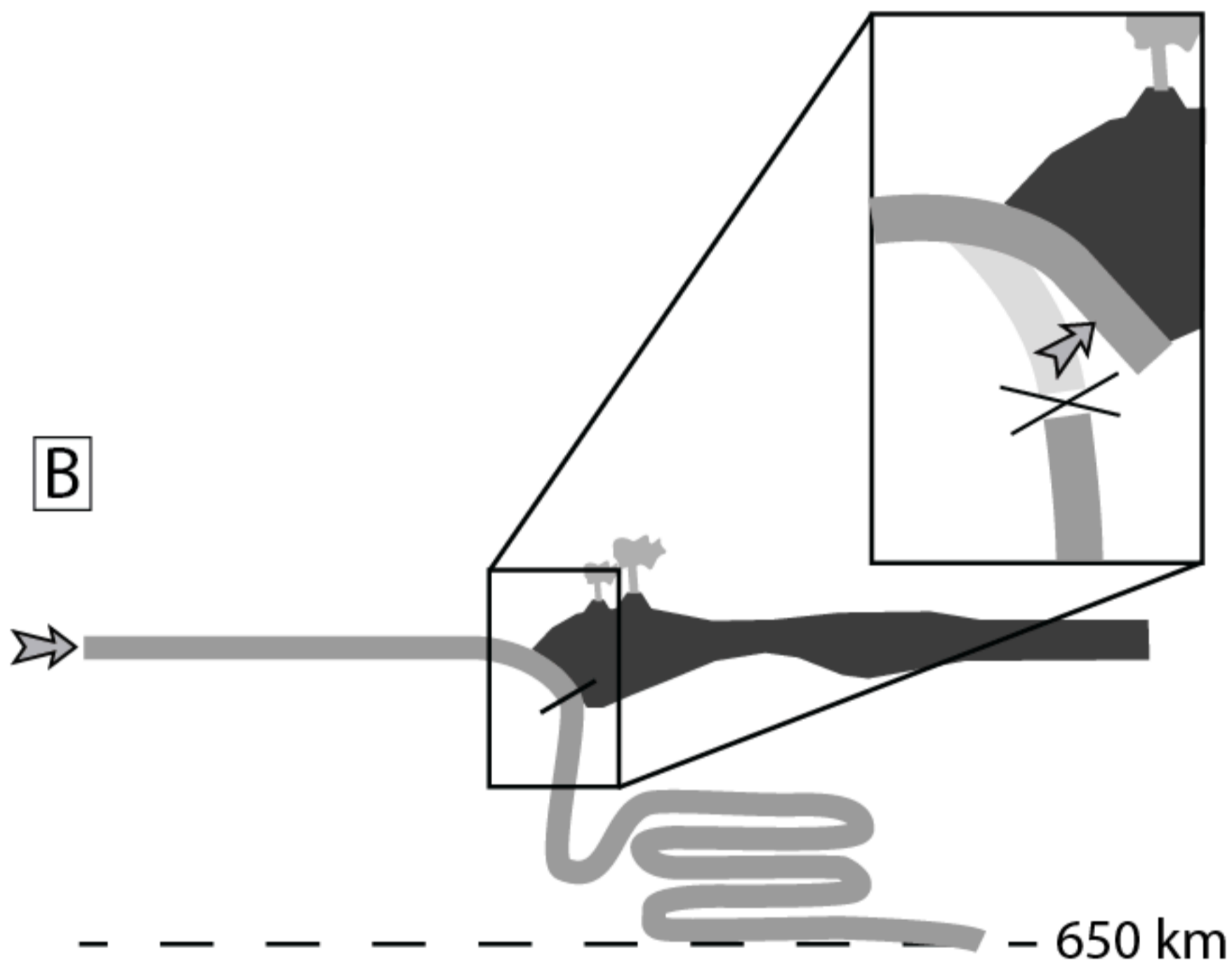
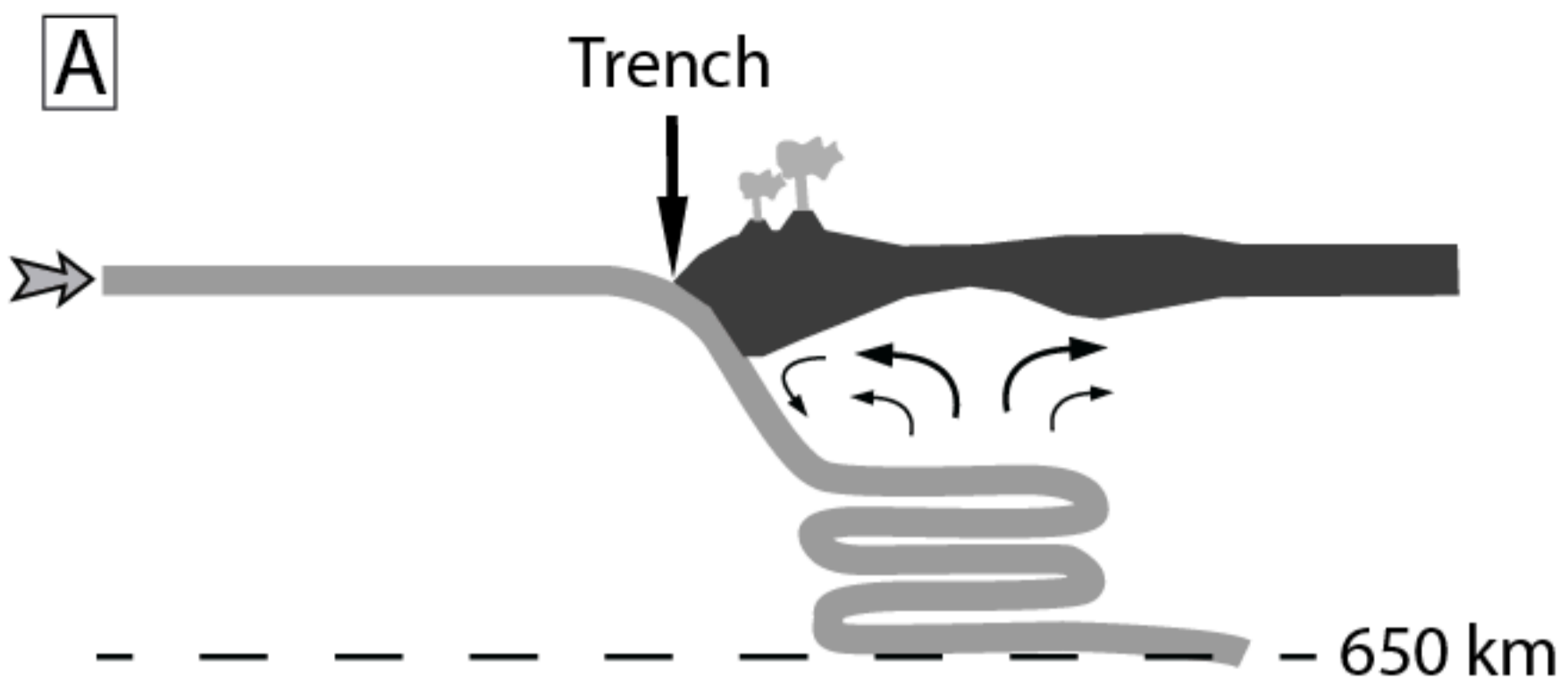




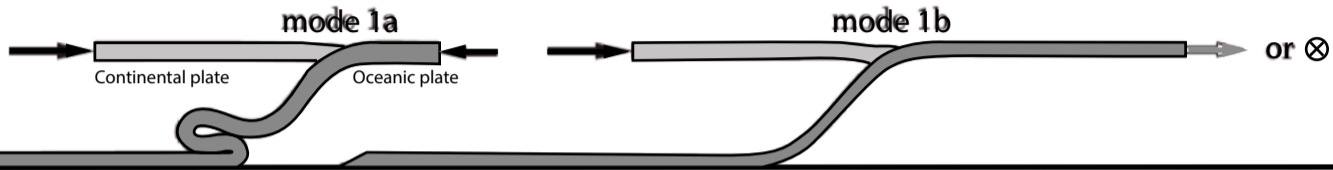








Case 1



Case 2

